TMED4 facilitates Treg suppressive function via ROS homeostasis in tumor and autoimmune mouse models

Zhenyan Jiang,[1] Huizi Wang,[1] Xiaoxia Wang,[1] Hongrui Duo,[2] Yuexiao Tao,[1] Jia Li,[1] Xin Li,[1] Jiamin Liu,[1] Jun Ni,[1] Emily Jiatong Wu,[1] Hongrui Xiang,[1] Chenyang Guan,[1] Xinyu Wang,[1] Kun Zhang,[3] Peng Zhang,[3] Zhaoyuan Hou,[4] Yong Liu,[5] Zhengting Wang,[6] Bing Su,[1] Bo Li,[2] Youjin Hao,[2] Bin Li,[1] Xuefeng Wu[1]

[1]Center for Immune-Related Diseases at Shanghai Institute of Immunology, Ruijin Hospital, Shanghai Jiao Tong University School of Medicine, Shanghai, China; Hongqiao International Institute of Medicine, Shanghai Tongren Hospital, Shanghai Jiao Tong University School of Medicine, Shanghai, China; Key Laboratory of Cell Differentiation and Apoptosis of the Chinese Ministry of Education, Shanghai Jiao Tong University School of Medicine, Shanghai, China; and Shanghai Institute of Immunology, Department of Immunology and Microbiology, Shanghai Jiao Tong University School of Medicine, Shanghai, China

[2] Research Group of Computational and Integrative Biology, College of Life Sciences, Chongqing Normal University, Chongqing, China

[3] Department of Pharmacology and Chemical Biology, Shanghai Key Laboratory of Emotions and Affective Disorders, Shanghai Jiao Tong University School of Medicine, Shanghai, China, 200025

[4] Department of Biochemistry and Molecular Cell Biology, Shanghai Key Laboratory for Tumor Microenvironment and Inflammation, Shanghai Jiao Tong University School of Medicine, Shanghai, China

[5]Hubei Key Laboratory of Cell Homeostasis, College of Life Sciences, Wuhan University, Wuhan 430072, China

[6]Department of Gastroenterology, Ruijin Hospital, Shanghai Jiao Tong University School of Medicine, Shanghai, China

Authorship note: ZJ, HW, Xiaoxia Wang, and HD contributed equally to this work.

Correspondence addressed to: haoyoujin@hotmail.com (YH), binli@shsmu.edu.cn (Bin Li), xuefengwu@shsmu.edu.cn (X. Wu)

Mailing address:

Dr. Youjin Hao, No. 37 Middle Road, University Town, Shapingba District, Chongqing, China. 401331, Tel: 86-23-65910315

Dr. Bin Li, No. 280 South Chongqing Road,Shanghai, China. 200025. Tel: +86-21-63846590-776783

Dr. Xuefeng Wu， No. 280 South Chongqing Road,Shanghai, China. 200025. Tel: +86-21-63846590-776684

Abstract

Endoplasmic reticulum stress (ERS) plays crucial roles in maintaining regulatory T cells (Treg) stability and function, yet the underlying mechanism remains largely unexplored. Here we demonstrate that ERS-related protein transmembrane p24 trafficking protein 4 (TMED4) Treg-specific knockout (*Tmed4*$^{\Delta Treg}$) mice contain more Treg cells with impaired Foxp3 stability, Treg signature and suppressive activity, which leads to T cell hyperactivation, exacerbated inflammatory phenotype and boosted anti-tumor immunity in mice. Mechanistically, loss of *Tmed4* causes defects in ERS and nuclear factor erythroid 2–related factor 2 (NRF2)-related antioxidant response, which results in excessive reactive oxygen species (ROS) that reduces Foxp3 stability and suppressive function of Treg cells in an IRE1α-XBP1 axis-dependent manner. The abnormalities can be effectively rescued by ROS scavenger, NRF2 inducer or forcible expression of IRE1α. Moreover, TMED4 suppresses IRE1α proteosome degradation via the ER-associated degradation (ERAD) system including BIP. Our study reveals that TMED4 maintains Treg cell stability and suppressive function through IRE1α-dependent ROS and the NRF2-related antioxidant response.

KEYWORDS

TMED4, Treg, Foxp3, IRE1α, ROS, ER stress, ERAD

INTRODUCTION

T regulatory cells (Treg), a distinct subset of $CD4^+$ T cells, perform an immunosuppressive function to maintain immunological homeostasis (1, 2). The transcription factor Foxp3 has been recognized as the leading signature gene and marker of Treg cells (3), reduced and unstable Foxp3 expression affects Treg cell differentiation and function (4). The inflammatory milieu in the tissue microenvironment and pharmacological molecules that induce chronic endoplasmic reticulum (ER) stress could damage Treg stability and convert them to T-effector-like phenotypes that encourage activation and expansion of autoreactive T cells and other innate immune cells (5-8). However, the mechanisms underlying how ER stress response regulates Foxp3 stability and Treg function remain elusive.

ER functions as the hub for the folding and quality control (QC) of secretory proteins, where misfolded proteins are primarily recognized by ER-associated degradation (ERAD) for proteasomal degradation (9, 10). Stress conditions in which mammalian cells are activated and increasingly require new protein synthesis can cause an accumulation of unfolded and misfolded proteins, identified by ER stress sensors inositol-requiring enzyme-1α (IRE1α), protein kinase R-like endoplasmic reticulum kinase (PERK) and activation of transcription factor 6 (ATF6) (11). IRE1α itself has been reported as an endogenous substrate for the ERAD complex that involves E3 ubiquitin ligase HRD1 and the unfolded protein response (UPR) chaperone BIP (12). However, the mechanism and function of ERAD-mediated degradation of IRE1α in Treg cells requires further investigation.

Several studies reveal functions of ER stress response in T cells (13-17), or Treg cells (8, 18). Unlike conventional $CD4^+$ T cells, Treg cells are mainly managed by mitochondrial oxidative phosphorylation (OXPHOS) for their bioenergetic needs (19-22). Dysregulated ER stress response and defects in mitochondrial OXPHOS are the main sources of cellular reactive oxygen species (ROS) (23, 24), which is subjected to clearance by nuclear factor erythroid 2-related factor 2 (NRF2), the best-described antioxidant transcription factor (25, 26). Adequate mitochondrial OXPHOS and ROS levels are critical for the regulation of Treg function (27-30), and it has been suggested that ER stress induced UPR is highly dependent on the redox signaling response (31). However, the crosstalk among the ER stress response, mitochondrial OXPHOS and antioxidant response in Treg cells remains elusive.

Yeast p24 protein can prevent misfolded proteins from entering vesicles secreted from the ER (32, 33). The human homolog of the p24 protein TMED4, namely ERS25 (ER stress response protein 25), is a potential ER stress response regulator (34). The ER Golgi transport inhibitor Brefeldin A induced TMED4 expression, indicating that TMED4 may act as a vesicular transport protein between the ER and Golgi apparatus.

In our study, we found that compared to their littermate controls, Treg cell specific *Tmed4* knockout mice (*Tmed4*$^{\Delta Treg}$) contain more Treg cells yet with lower Foxp3 expression and impaired suppression activity. *Tmed4*$^{\Delta Treg}$ mice exhibit exacerbated symptoms in EAE, chronic colitis models and boosted antitumor immunity. Loss of TMED4 in Treg cells leads to defects in homeostasis of the ER stress response and mitochondria integrity, which cause accumulated cellular ROS, and subsequently

impairs Foxp3 stability and suppressive function of Treg cells which can be restored by the ROS scavenger, NRF2 inducer or expression of IRE1α. Collectively, TMED4 regulates Treg cells stability and suppressive function by sustaining IRE1α-dependent regulation of cellular ROS and NRF2-realated antioxidant response, and TMED4 suppress IRE1α proteosome degradation via ERAD system including BIP.

RESULTS

Treg cell specific *Tmed4* knockout (*Tmed4*$^{\Delta Treg}$) mice exhibit T cell hyper-activation, and impaired Foxp3 stability in Treg cells

Within the tumor microenvironment, ER stress plays a complex role in the balance between antitumor activities of immune cells and tumor cell adaptation and escape, in which innate immunosuppressive profiles of Treg cells can be reprogrammed to disturb their antitumor effect (35). We speculate that suppressive activity of tumor infiltrating Treg cells correlates with their intrinsic ER stress responses. To identify the potential influence of TMED4 on the regulatory function of Treg cells within the tumor microenvironment, we conducted correlation analyses on the gene expression profiles obtained from various cancer datasets including colon (COAD), rectal (READ), lung adenocarcinomas (LUAD), liver (LIHC), and gastric cancers (STAD) sourced from The Cancer Genome Atlas (TCGA). We found a strong positive correlation between the expression profiles of ER stress response-associated genes and *TMED4* (Supplemental Figure 1A), suggesting that TMED4 may regulate ER stress response within the tumor

microenvironment. Additionally, we observed a significant positive correlation between the expression profiles of Treg signature genes and *TMED4* (Supplemental Figure 1B). To verify these findings, we sorted $CD4^{+}CD25^{high}$ Treg cells from human colorectal, gastric and renal cancer samples for the correlation analyses of mRNA expression. Indeed, we observed that the *TMED4* mRNA expression positively correlated with that of *HSPA5* and *DDIT3*, which reflect activation of the unfolded protein response (UPR) (Supplemental Figure 1C). We further identified positive correlations between expression levels of *TMED4*, *DDIT3*, or *HSPA5* (not significant but correlation tendency) with *FOXP3* (Supplemental Figure 1D). The above evidence suggests that TMED4 positively correlates with ER stress responses and FOXP3 expression of the tumor infiltrating Treg cells. This promoted us to further investigate the involvement of TMED4 in regulating suppressive functions of Treg cells and how this may affect antitumor activity through ER stress responses.

We first generated Treg cell specific knockout mice ($Tmed4^{\Delta Treg}$, also designated as cKO) by crossing *Foxp3-Cre* mice with $Tmed4^{f/f}$ mice, whose Treg cells were confirmed efficient deletion of TMED4 in both protein and mRNA (Supplemental Figure 2, A and B). $Tmed4^{\Delta Treg}$ mice started to show spontaneous inflammation and a propensity for autoimmunity as early as 12-week-old. Compared to their $Tmed4^{f/f}$ littermate controls, $Tmed4^{\Delta Treg}$ mice exhibited splenomegaly, lymphadenopathy, lower body weight and increased lymphocytic infiltration in non-lymphoid organs, particularly in the lungs (Figure 1, A and B, and Supplemental Figure 2C). Under resting conditions, spleens, peripheral lymph nodes (pLNs) and lungs of $Tmed4^{\Delta Treg}$ mice

contained higher percentages of $CD4^+CD44^{hi}CD62^{lo}$ and $CD8^+CD44^{hi}$ effector T cells than their littermate WT control mice (Figure 1, C-E). In addition, *Tmed4*$^{\Delta Treg}$ mice had markedly higher frequencies of IFN-γ-producing $CD4^+$ and $CD8^+$ T cells in the spleens and pLNs than *Tmed4*$^{f/f}$ mice (Figure 1, F and G). Furthermore, *Tmed4*$^{\Delta Treg}$ mice contained a relatively higher percentage of neutrophils ($CD11b^+Ly6G^+$) in the spleen than *Tmed4*$^{f/f}$ mice (Figure S2D). Thus, TMED4 deficiency in Treg cells resulted in T cell hyperactivation and inflammatory phenotype in mice.

We further investigated how TMED4 regulates functions of Treg cells. Compared to their littermate controls, *Tmed4*$^{\Delta Treg}$ mice contained higher percentages of Treg cells in the spleens, pLNs and lungs (Figure 1, H and I). In vitro assay showed splenic *Tmed4*-deficient Treg cells were hyper-proliferative, despite with similar $Ki67^+$ levels to WT controls (Supplemental Figure 2, E and F). The apoptosis ratios of Treg cells from the spleens of both genotypes were comparable when assessed using annexin V antibodies (Supplemental Figure 2, G and H), suggesting that increased frequency of Treg cells in *Tmed4*$^{\Delta Treg}$ mice may not be due to impairment in their ability to proliferate and survive, but impairment in immunosuppressive function of Treg cells which triggered a compensatory increase of Treg cells number in vivo. To further understand the intrinsic alterations in the stability and function of *Tmed4*-deficient Treg cells, we found that the mean fluorescence intensity (MFI) of Foxp3 was reduced in KO Treg cells from spleens, pLNs and lungs (Figure 1J). In addition, induction of purified naïve $CD4^+$ T cells using Treg differentiation supplements for two and three days revealed that Foxp3 expression was lower in KO iTreg cells compared to WT cells (Figure 1, K

and L). Then we measured FOXP3 protein decay by cycloheximide (CHX) treatment in mouse primary Treg cells and found that the protein stability of FOXP3 in *Tmed4*-deficient Treg cells was markedly reduced (Figure 1, M and N). In conclusion, TMED4 plays a pivotal role in the maintenance of homeostasis and suppressive function of Treg cells.

Tmed4 deficiency alters Treg cells' signature profiles in a cell intrinsic manner

To systematically investigate the effect of *Tmed4* deficiency on Treg cell homeostasis and function, we performed RNA-sequencing analysis on in vitro activated Treg cells, which showed differentially expressed genes in *Tmed4*-deficient Treg cells (Figure 2A, 55 upregulated and 100 downregulated). Particularly, we found significantly enhanced expression of genes reflecting effector T cell function and differentiation such as *Gzma*, *Gzmb*, *Il6*, *Il17f*, *Il13*, and *Ccl3* in KO Treg cells (Figure 2B). Meanwhile, the signature genes reflecting Treg cells stability and function were markedly downregulated in the *Tmed4*-deficient group (Figure 2, C and D). Since *Tmed4* deletion impaired the stability of Foxp3, we subsequently confirmed that the absence of *Tmed4* also downregulated the immunosuppressive function of Treg cells against T cell proliferation by in vitro suppression assays (Figure 2, E and F). We also found that the MFI of CD25, a key molecule that characterizes Treg cells, was reduced in the spleens, pLNs and lungs of KO Treg cells (Figure 2G)

To rule out the possible influence of extrinsic inflammation on Treg cells in vivo, we generated bone marrow chimera mice in which the recipient CD45.1$^+$ mice were subjected X-ray irradiation to eliminate hematopoietic cells and reconstituted by a

mixture of bone marrow cells from CD45.1/CD45.2$^+$ *Tmed4*$^{f/f}$ mice and CD45.2$^+$ *Tmed4*$^{\Delta Treg}$ mice. In these mice, Treg cell percentages were comparable (Figure 2, H and I), and expression levels of representative surface markers of Treg cell, including Foxp3, CD25, CTLA4 and GITR in *Tmed4*-deficient Treg cells were all reduced compared to WT counterparts (Figure 2, J and K). Particularly, *Tmed4*-deficient Treg cells expressed higher PD1, which is generally considered to be negatively correlated with suppressive function (36). While the upregulation of CD69 showed higher activation of *Tmed4*-deficient Treg cells, OX40 and ICOS were down-regulated (Supplemental Figure 3, A and B). To further determine whether TMED4 regulates Treg cell homeostasis in a cell-intrinsic manner, we took advantage of *Tmed4*$^{f/f}$*Foxp3*$^{Cre/+}$ female mice (designated as chimera mice), in which around half of the Treg cells are TMED4-sufficient (without *Foxp3*-driven YFP-Cre fusion protein expression, designated as YFP$^-$ Treg), while the other half of the Treg cells are *Tmed4*-deficient (with Foxp3-driven YFP-Cre fusion protein expression, designated as YFP$^+$ Treg) due to random X chromosome inactivation (37). In both *Tmed4*$^{+/+}$*Foxp3*$^{Cre/+}$ (both YFP$^-$ and YFP$^+$ Treg cells were *Tmed4*-sufficient) and chimera mice, although the proportion of YFP$^+$ Treg cells was lower than that of YFP$^-$ Treg cells (Figure 2, L and M), the relative ratios of YFP$^+$ to YFP$^-$ were similar between the two groups (Figure 2N), suggesting that loss of *Tmed4* did not affect the proliferative properties of Treg cells in the chimera mice. While the expression of Foxp3 as well as CD25, CTLA4 and GITR were significantly down-regulated only in the chimera YFP$^+$ Treg cells (Figure 2O and Supplemental Figure 3C). Taken together, it suggested that *Tmed4*-deficient Treg cells

exhibit effector phenotype and reduced signature profiles in a cell-intrinsic manner.

Loss of *Tmed4* in Treg cells leads to more exacerbated inflammatory phenotype and boosted anti-tumor immunity in mice

To investigate the in vivo pathophysiological consequences of *Tmed4* ablation in Treg cells, we utilized an EAE (experimental autoimmune encephalomyelitis) mouse model. In this model, mice will exhibit clinical EAE scores upon MOG (myelin oligodendrocyte glycoprotein) peptide immunization. In the parallel treatment groups, $Tmed4^{\Delta Treg}$ mice developed more severe disease symptoms than their littermate $Tmed4^{f/f}$ control mice 11 days after immunization (Figure 3A and Supplemental Figure 4A), along with higher proportions of $CD4^+$ and $CD8^+$ T cells infiltrating in the central nervous system (CNS) (Figure 3B). Through H&E staining and LFB (Luxol fast blue) histological staining analysis, we confirmed that $Tmed4^{\Delta Treg}$ mice contained more CNS-infiltrating immune cells and more severe demyelination than $Tmed4^{f/f}$ group (Figure 3C). Consistent with results from resting conditions, the draining lymph node (dLN) and CNS of $Tmed4^{\Delta Treg}$ mice contained higher frequencies of Treg cells, but with lower Foxp3 expression than that of their $Tmed4^{f/f}$ controls (Figure 3, D and E, and Supplemental Figure 4B). Consequently, the percentages of IFN-γ-secreting $CD4^+$ or $CD8^+$ T cells, and IL-17-secreting $CD4^+$ T cells were also higher in both dLN and CNS of $Tmed4^{\Delta Treg}$ mice (Figure 3, F and G, Supplemental Figure 4, C and D).

We further utilized a T cell transfer colitis model in which naïve T cells administered to the lymphopenia $Rag1^{-/-}$ mice results in severe colitis, while co-transfer of naïve T cells together with Treg cells attenuated the severity of colitis (38). $Rag1^{-/-}$

mice transferred with naïve T cells and *Tmed4*-deficient Treg cells failed to prevent progressive body weight loss as seen with that of co-transferring naïve and WT Treg cells group (Figure 3H), the latter group also exhibited less intestinal damage as shown by H&E histological analysis (Figure 3I), and significantly less inflammatory cell infiltration in both colon and small intestine (Figure 3J). To rule out role for mutant Treg cells in the development of the disease, we injected WT Treg and KO Treg cells alone into *Rag1*$^{-/-}$ mice and found that neither group induced significant colitis as CD4^{+} T cell injection did (Supplemental Figure 4E).

Since the manifestation of TMED4 significantly associates with Foxp3 in human tumors, we proceeded to investigate how TMED4 regulates Treg cell-mediated anti-tumor immunity. The colorectal cancer MC38 cells inoculated into *Tmed4*$^{\Delta Treg}$ mice had significantly slower growth kinetics and ended up with smaller tumor sizes compared with that of their littermate controls (Figure 4A). Consistently, T cell activation was significantly higher in lymphoid organs, particularly in dLN of *Tmed4*$^{\Delta Treg}$ mice (Supplemental Figure 5, A-D). The proportion of tumor-infiltrating Treg cells was higher in tumor-bearing *Tmed4*$^{\Delta Treg}$ mice (Figure 4B and Supplemental Figure 5E), whose Treg cells derived from dLN and tumor had significantly lower Foxp3 expression levels (Figure 4C). Intracellular staining (ICS) revealed significantly higher or higher tendency of production of IFN-γ (Figure 4, D and E, and Supplemental Figure 5F) and TNF-α (Figure 4, F and G, and Supplemental Figure 5G) by T cells, especially in tumor-infiltrating T cells derived from *Tmed4*$^{\Delta Treg}$ mice. The results also showed that tumor-infiltrating Treg cells derived from *Tmed4*$^{\Delta Treg}$ mice secreted more IFN-γ but no

differences in IL-17 (Figure 4H and Supplemental Figure 5H). Collectively, loss of *Tmed4* in Treg cells leads to more exacerbated inflammatory phenotype and boosted anti-tumor immunity in mice.

***Tmed4*-deficiency leads to impaired ER stress response, mitochondria integrity and accumulated ROS in Treg cells**

Given that TMED4 functions as an ER stress response protein and imbalanced ER stress response would cause Treg cells instability and dysfunction (8, 34), we set out to investigate how TMED4 may regulate ER stress responses in Treg cells. We induced ER stress in vitro by using thapsigargin (TG), an inhibitor of microsomal Ca^{2+}-ATPase. Upon TCR and ER stress induction, UPR activation hallmark genes *Bip* and *Chop* were significantly upregulated in the WT Treg cells, yet the extent of induction was dramatically decreased in *Tmed4*-deficient Treg cells (Figure 5A). Importantly, *Tmed4*-deficiency in Treg cells led to significantly downregulation of IRE1α protein level and XBP1 spliced form XBP1s, while ATF6N (cleaved N-terminus of ATF6, representing its activated form) and PERK were only slightly reduced or unchanged (Figure 5B). In keeping with reduction of IRE1α protein levels, *Tmed4*-deficient Treg cells also exhibited lower IRE1α phosphorylation and TRAF2 protein levels (Supplemental Figure 6A). In addition to the typical ERS markers, the transcription levels of *Xbp1* downstream target genes *Erdj4*, *Sec61a1* and PERK downstream gene *Atf4* were all significantly downregulated (Figure 5, C-E).

ER stress could affect many facets of mitochondrial functions, through which the IRE1α and PERK arms could have impact on mitochondrial bioenergetics and

regulation of proteostasis by mitochondrial quality control (39-41). Recent studies have shown that ER dysfunction can raise the calcium and oxidative load in the ER and mitochondria, leading to mitochondrial dysfunction (23, 31). KEGG and GO analysis showed genes associated with activation of immune response pathways were upregulated, while vesicle transport and antioxidant response pathways in *Tmed4*-deficient Treg cells were downregulated (Figure 5F). Seahorse analysis showed decreased oxygen consumption rates (OCR) in KO Treg cells (Figure 5, G and H), indicating a deficit in capacity of mitochondrial activity. In addition, higher degree of mitochondria damage was detected in KO Treg cells as shown by Mito-Tracker FCM staining (Supplemental Figure 6B). Interestingly, we found upregulation of extracellular acidification rate (ECAR) levels in *Tmed4*-deficient Treg cells (Supplemental Figure 6, C and D), which also had higher levels of mTOR phosphorylation and downstream S6 phosphorylation as shown by FCM analysis (Supplemental Figure 6, E and F). The above phenotypes suggested that *Tmed4*-deficient Treg cells may compensate for OXPHOS defects due to mitochondrial damage by glycolysis, and cell proliferation was facilitated by up-regulation of mTOR pathway activity at the cost of Foxp3 expression and suppressive function, which matched a previous report (42).

Cellular imbalance of redox homeostasis caused by dysregulation of ER stress response and mitochondrial integrity leads to excessive accumulation of intracellular ROS, the well-recognized key factor affecting the biological processes of Treg cells and can further regulate their immunosuppressive functions (27, 28). The production of

ROS by mitochondria is modulated by complex I and complex III, which contribute to both oxidative respiration and the clearance of ROS generated from the mitochondrial electron transport chain (43). Analysis of RNA-seq data revealed that expression levels of different components of mitochondrial complex genes were decreased in *Tmed4*-deficient Treg cells (Supplemental Figure 6G). We also validated the defect in expression of several pivotal genes of mitochondrial complexes I and III, including *mt-Cytb*, *mt-Nd1*, and *mt-Nd4* in *Tmed4*-deficient Treg cells (Figure 5, I-K). The activation of antioxidant response, which is responsible for scavenging ROS, is dominantly facilitated by NRF2 (24, 44), known as a PERK substrate (45), along with factors associated with antioxidant response. Correspondingly, we found a significant positive correlation between upregulation of TMED4 and activation of antioxidant response in the tumor microenvironment, as obtained from the TCGA datasets (Supplemental Figure 6H). PERK downstream kinase activity indicated by eIF2α phosphorylation, and NRF2 protein levels were also significantly reduced (Figure 5L). Concomitantly, the mRNA levels of NRF2 downstream genes *Gclm* and *Ho-1* were also drastically reduced in *Tmed4*-deficient Treg cells (Supplemental Figure 6, I and J). Next, we set out to detect mitochondrial ROS and cellular total ROS in splenic Treg cells through Mito-SOX and CFDA staining, respectively. The results showed higher expression level of mitochondrial ROS and total ROS upon TCR stimulation and a more dramatical increase when ERS was induced in *Tmed4*-deficient Treg cells (Figure 5, M-O). Collectively, TMED4 maintains ER stress response, mitochondrial integrity, and ROS homeostasis in Treg cells.

ROS scavenger or NRF2 inducer restores Foxp3 expression and suppressive function of *Tmed4*-deficient Treg cells

Tmed4-deficiency led to ROS accumulation and impaired antioxidant response in Treg cells. It is therefore important to determine whether directly scavenging cellular ROS or restoring NRF2 activity could affect cellular phenotypes of *Tmed4*-deficient Treg cells. We treated WT and *Tmed4*-deficient splenic Treg cells with NAC, a common ROS scavenger and found that the differences in ROS levels between these two genotypes of Treg cells were significantly erased (Figure 6, A and B). TG-induced ER stress promotes Treg cell suppressive activity and Foxp3 expression to a certain extent (46). Foxp3 expression level in *Tmed4*-deficient Treg cells was achieved by NAC plus TG treatment, but not by NAC alone (Figure 6C). The same effect was achieved by NRF2 inducer sulforaphane (Supplemental Figure 7, A-C), which could restore NRF2 level in *Tmed4*-defcient Treg cells similarly to that of WT Treg cells (Supplemental Figure 7D). Interestingly, expression of Foxp3 in cells treated with higher doses of NAC (5 mM compared to 1 mM) was not replenished but contrarily decreased in the presence of TCR stimulation alone, while Foxp3 expression was better replenished when the ER stress was induced (Supplemental Figure 7, E and F). This finding indicates that appropriate ROS levels are essential for the maintenance of Foxp3 expression in Treg cells. To further examine whether modulating ROS level could erase the difference in suppressive function of WT and *Tmed4*-deficient Treg cells both in vitro and in vivo, we first performed an in vitro suppression assay and found that the suppressive function of WT and *Tmed4*-deficeint Treg cells were both rescued to the same level (Figure 6,

D and E). Meanwhile, we examined the level of cellular ROS and found that NAC pretreatment could have a lasting suppressive effect on cellular ROS levels (Supplemental Figure 7, G and H). Additionally, we carried out in vivo rescue experiments in which WT or *Tmed4*-deficient CD45.2$^+$ Treg cells pretreated with DMSO and NAC, respectively were inoculated into MC38 tumor cell-bearing CD45.1$^+$ mice. Two consecutive inoculations of Treg cells subjected to these different treatments were i.v. injected on day 0 and 7 (working model was shown in Supplemental Figure 8A). Tumor growth differences between the *Tmed4*$^{f/f}$ and *Tmed4*$^{\Delta Treg}$ treated with DMSO were eliminated by treatment with NAC (Figure 6F and Supplemental Figure 8B). Further, we found that the activation of host CD4$^+$ and CD8$^+$ T cells in the NAC pretreated group was effectively rescued, not only downregulation of the proportion of effector cells, but also secretion of IFN-γ (Figure 6, G-I, and Supplemental Figure 8, C-E). In addition, both percentages of IFN-γ or IL-17-secreting Treg cells in the group that was inoculated with NAC treated were significantly decreased compared to that of non-treated *Tmed4*-deficient Treg cells (Figure 6J and Supplemental Figure 8F). Meanwhile, the results of the cellular ROS level showed that NAC could still provide sustained suppression of the cellular ROS after 7-day pretreatment (Supplemental Figure 8, G and H). The above results demonstrated that cellular ROS scavenger or NRF2-activation restored the expression level of Foxp3 and the suppressive activity of *Tmed4*-deficient Treg cells both in vitro and in vivo.

Tmed4-deficiency in Treg cells leads to lower Foxp3 expression and ROS accumulation in an IRE1α-XBP1 axis dependent manner

Given that deletion of *Tmed4* leads to substantial decrease in IRE1α protein levels, along with downstream RNase splicing and kinase activities, and lower NRF2 protein levels, we proceeded to investigate the prevailing cause governing the regulation of Treg function. To this end, we generated IRE1α Treg specific knockout mice (*Ern1*$^{\Delta Treg}$). Importantly, *Ern1*$^{\Delta Treg}$ mice generally phenocopied *Tmed4*$^{\Delta Treg}$ mice, *i.e.*, IRE1α-deficiency in Treg cells led to hyper-activation of $CD4^+$ and $CD8^+$ T cells, as well as the ability to secrete more IFN-γ in $CD4^+$ T cells from the KO group (Figure 7, A and B, and Supplemental Figure 9, A and B). Consistent with *Tmed4*$^{\Delta Treg}$ mice, *Ern1*-deficient Treg cells gained effector functions and secreted more IFN-γ (Figure 7C and Supplemental Figure 9C). Loss of *Ern1* led to accumulated cellular and mitochondrial ROS levels compared to the WT Treg cells (Figure 7, D and E, and Supplemental Figure 9D), along with lower Foxp3 expression levels (Figure 7F and Supplemental Figure 9D). Compared to WT Treg cells, *Ern1*-deficient Treg cells had defect in suppressive function (Supplemental Figure 9, E and F). We further dissected whether RNase splicing or kinase activity of IRE1α is more critical in determining Treg cells suppressive function by applying IRE1α RNase splicing activity inhibitor 4μ8C or kinase activity inhibitor KIRA6 respectively. Upon 4μ8C, but not KIRA6 treatment in Treg cells, led to remarkable reduction of cellular Foxp3 expression and accumulated ROS levels (Figure 8, A and B, and Supplemental Figure 9G). Serving as controls, parallel experiments showed both inhibitors functioned well (Supplemental Figure 9, H-J).

On the other hand, we examined whether complementing IRE1α could restore

suppressive function of *Tmed4*-deficient Treg cells. To this end, we forcibly expressed IRE1α in *Tmed4*-deficient iTreg cells through infecting them with Sindbis virus carrying *Ern1* cDNA, followed by confirming IRE1α protein expression (Supplemental Figure 10A). Importantly, IRE1α expression could restore cellular levels of XBP1s or Foxp3 expression, and suppress ROS levels, respectively (Figure 8, C and D, and Supplemental Figure 10B), along with their in vitro suppressive function (Figure 8, E and F).

Loss of *Tmed4* in Treg cells partially downregulated p-eIF2α-NRF2, an axis that lays downstream of PERK (Figure 5L). Therefore, we set out to investigate whether the PERK pathway would independently affect cellular ROS levels and Foxp3 expression. The PERK kinase activity inhibitor GSK2656157, which effectively suppresses the PERK pathway (Supplemental Figure 10C), and concomitant with notably lower level of NRF2 expression, did not cause significant change in Foxp3 expression levels in Treg cells, despite of a slight upregulation of ROS levels (Supplemental Figure 10, D-F). To validate above conclusions more directly, we silenced PERK protein expression in iTreg cells induced in vitro by siRNA (Supplemental Figure 10G). Upon PERK silencing, TG-induced ER stress still up-regulated cellular ROS levels, but did not down-regulate Foxp3 expression (Supplemental Figure 10, H and I), suggesting that lower Foxp3 expression in *Tmed4*-deficient Treg cells was not caused by down-regulation of PERK pathway. Interestingly, *Ern1*-deficiency did not change protein abundancies of PERK, NRF2, and TMED4 in Treg cells under resting or ER stress condition (Figure 8G). Taken together, *Tmed4*-deficiency in Treg cells led to lower

Foxp3 expression and ROS accumulation in an IRE1α-XBP1 axis dependent manner.

TMED4 suppresses HRD1/BIP-mediated IRE1α degradation

Given that downregulation of IRE1α protein levels is the leading cause for impaired function of *Tmed4*-deficient Treg cells, we proceeded to reveal the regulatory mechanisms through which TMED4 impacts the expression of IRE1α protein. When ER stress is present, IRE1α forms dimers to activate downstream ER stress response. However, this process can be reversed by BIP overexpression, allowing more IRE1α degradation by the ERAD complex involving HRD1(12). In 293T cells, TMED4 overexpression inhibited BIP-induced IRE1α degradation (Figure 9, A and B). We further identified that TMED4 interacts with IRE1α and BIP (Figure 9, C and D). Besides, upon induction of ER stress, these three proteins exhibited enhanced binding with one another (Figure 9, D and E), suggesting that TMED4 facilitated stabilization and function of IRE1α during ER stress, in which BIP might serve as a bridge, mediating binding of IRE1α to ERAD complex. TMED4 overexpression alone, regardless ER stress induction, led to IRE1α dissociation from HRD1 (Figure 10A). Moreover, TMED4 remarkably inhibited HRD1-mediated K48 polyubiquitination of IRE1α (Figure 10B). In the in vitro induced mouse iTreg cells, *Tmed4*-deficiency increased K48-linked ubiquitination of IRE1α (Figure 10C), providing evidence of TMED4-mediated degradation of IRE1α in primary cells. Therefore, the above results implied TMED4 stabilizes IRE1α through blocking BIP-mediated ERAD system degradation process in Treg cells.

DISCUSSION

In this study, we demonstrate that *Tmed4* deficiency not only leads to the loss of ER homeostasis in Treg cells, but also results in defective mitochondrial activity and excessive accumulation of cellular ROS, which in turn affects cellular metabolic processes and redox signaling homeostasis, consequently causing downregulation of Foxp3 stability and impaired suppressive functions. Specifically, TMED4 protects Treg cells from oxidative stress by maintaining IRE1α protein level and the equilibrium of the IRE1α-XBP1 axis.

ROS sustains cell survival or death process by mediating cell signaling pathways and transcription factors via activation of NRF2-associated pathway signals (31). Conventionally, mitochondria have been recognized as the main location of cellular ROS generation. With several recent studies demonstrating that under stressful circumstances, ER luminal ROS levels also increase, and consequently, release of calcium and peroxide into the cytosol disrupts the mitochondrial redox reaction (47). In our study, we found that TCR stimulation led to mitochondrial functional defects in Treg cells due to *Tmed4* loss, but mitochondrial ROS levels remained unaffected. However, these defects were exacerbated by ER stress, indicating delayed ROS production in mitochondria. We suggest that *Tmed4* deficiency may cause ER defects that precede mitochondrial morphological and functional issues in Treg cells. Further investigation is needed to understand the complex interplay between ER stress and antioxidant responses in immune cell function, particularly Treg cells. It is suggested that the regulation of ROS levels in Treg cells is not simply binary; an optimal threshold

is essential for maintaining their normal and stable functions under stress or pathological conditions.

Tmed4 deficiency shifts cellular metabolism towards glycolysis over OXPHOS, highlighting the need to investigate its role in the redox metabolic network, particularly in the ER, and its involvement in key substrate dynamics. Glutathione (GSH) deficiency in Treg cells, a vital antioxidant for redox homeostasis, produces phenotypes similar to TMED4 deficiency, enhancing cell proliferation and activation while reducing Foxp3 expression and suppressive function (48). This suggests TMED4's potential in regulating ER stress responses and the metabolic network supporting antioxidant functions. Further research is needed to clarify whether TMED4 affects the synthesis and degradation of key redox metabolites like GSH, impacting cellular ROS levels and functional stability.

Both the UPR and ERAD processes are evolutionarily conserved quality control systems crucial for maintaining ER homeostasis (49). This balance affects the dynamic activity of IRE1α. In the IRE1α degradation model, BIP acts as a bridge for its interaction with the ERAD complex. The stronger interaction between TMED4 and IRE1α upon BIP overexpression suggests that further investigation is needed to determine if BIP also regulates IRE1α degradation by TMED4, facilitating its dissociation from the ERAD complex and subsequent dimerization to activate downstream UPR signaling pathways. Additionally, the potential role of TMED4 as a chaperone in the UPR, working with BIP to maintain overall ER homeostasis, warrants thorough exploration.

The absence of TMED4 facilitates the conversion of Treg cells to Teff cells, enhancing T cell activation and anti-tumor immunity in the MC38 tumor model. Sustained ER stress in the tumor microenvironment hampers the function of tumor-infiltrating T cells. In ovarian cancer, the lack of the IRE1α-XBP1s signaling axis has been shown to boost T cell anti-tumor activity and prolong host survival (50, 51). Silencing this axis in Treg cells by suppressing TMED4 may enhance overall T cell anti-tumor activity across different tumors. Additionally, CHOP deletion has been linked to increased anti-tumor activity of $CD8^+$ T cells by promoting T-bet expression (52). Our findings indicate that TMED4 deficiency reduces CHOP levels in Treg cells, promoting their conversion to Teff cells and enhancing the activity of other T cell subsets, particularly Th1 and $CD8^+$ T cells, though the direct connection remains to be explored. The UPR protein PERK, while not directly involved in our system, also influences CHOP and NRF2 regulation. Understanding the relationship between TMED4 and the PERK regulatory network in managing ROS levels and cellular functions will be essential for clarifying how ER stress responses affect Treg cells and contribute to anti-tumor immunity.

In summary, our findings underly the importance of TMED4 in Treg homeostasis and its role in maintaining ER stress response and mitochondrial activity to avoid impairment of Treg Foxp3 expression and cellular function caused by excessive accumulation of cellular ROS. TMED4 serves as a rheostat balancing ER stress response and redox signaling pathway. These observations advance our understanding of the role TMED4 plays in Treg cells in alleviating autoimmune diseases and

enhancing anti-tumor immunity.

METHODS

Sex as a biological variant

We included both male and female sexes in human samples' collection and study, and sex was not considered as a biological variable. Except for the female chimera experiment, our study examined male mice.

Mice

CD45.1 mice were from Jackson laboratory and generously provided by Dr. Jinke Cheng at Shanghai Jiao Tong University School of Medicine. *Tmed4*$^{\Delta Treg}$ and *Ern1*$^{\Delta Treg}$ mice were obtained by crossing *Foxp3-YFP-Cre* mice(from Jackson laboratory) (53) with *Tmed4*$^{f/f}$ and *Ern1*$^{f/f}$ mice that were generated by Shanghai Biomodel Organism Science Technology Development Co., Ltd and generally provided by Dr. Yong Liu (Wuhan University, China) respectively (54). *Rag1*$^{-/-}$ mice were purchased from Cyagen Biosciences (Suzhou, China). All mice used for experiments were on a C57BL/6 background and 12-16 weeks of age except for the use of 8-week-old *Rag1*$^{-/-}$ mice at the time of the experiments. All mice were kept in a specific pathogen-free facility, and all mouse experiments were conducted following protocols approved by the Institutional Animal Care and Use Committee of Shanghai Jiao Tong University School of Medicine.

Patients and specimens

Tumor specimens were obtained and processed as previously described (55). Briefly, tumor tissues were dissociated mechanically and enzymatically using Collagenase D (Sigma) and DNase I (Sigma) for further isolation of tumor-infiltrating Treg cells. Mononuclear cells were then isolated by a Ficoll-Hypaque gradient (GE healthcare). Isolation of $CD4^+CD25^{high}$ Treg cells was achieved using flow cytometry sorting. RNA was quickly extracted with TRIZOL reagent (Invitrogen), reverse-transcribed, and analyzed by qRT-PCR.

Cell culture and sorting

HEK293T cell line was purchased from ATCC and cultured in DMEM supplemented with 10% FBS, 40 μM L-glutamine (STEMCELL) and 1% penicillin and streptomycin. Unless otherwise noted, all lymphocytes were isolated from spleens and pLNs (axillary and inguinal lymph nodes included), from where naïve $CD4^+$ cells ($CD4^+CD44^{low}CD62L^{high}$) or $CD4^+CD25^{high}$ Treg cells were separated using kits (STEMCELL) respectively and cultured in RPMI 1640 media supplemented with 10% FBS (GIBCO), 50 μM β-mercaptoethanol (Sigma) and 1% penicillin and streptomycin. α-CD3 (1 μg/mL) and α-CD28 (1 μg/mL) antibodies were used to stimulate purified Treg cells in 96-well round bottom microplates (about 2×10^5 cells per well) for flow cytometry, IB, qRT-PCR, or RNA-seq analysis. For in vitro iTreg cells induction, 48-well plates coated with α-CD3 (1 μg/mL) and α-CD28 (1 μg/mL) antibodies were used and naïve $CD4^+$ cells were isolated from mice spleen cells in the presence of ImmunoCultTM Mouse Treg Differentiation Supplement (STEMCELL), 10% FBS,

100 μM HEPES Buffer Solution (STEMCELL), 40 μM L-Glutamine (STEMCELL), 100 μM MEM Non-Essential Amino acids Solution (STEMCELL), 1 mM Sodium Pyruvate (Thermo Fisher), 50 μM β-mercaptoethanol (Sigma), 1% penicillin and streptomycin in RPMI 1640 medium for 2-6 days.

METHOD DETAILS

Tumor models

Mouse colon cancer (MC38) cells were cultured in RPMI 1640 supplemented with 10% FBS and These tumor cells were injected subcutaneously into 8-week-old *Tmed4*$^{f/f}$ and *Tmed4*$^{f/f}$*Foxp3-Cre* mice (5×10^5 cells per mouse). In the adaptive transfer model, purified 2×10^6 Treg cells from *Tmed4*$^{f/f}$ and *Tmed4*$^{\Delta Treg}$ mice donor mice were co-injected subcutaneously into CD45.1 recipient mice with 5×10^5 MC38 cells. After tumor inoculation, a second dose of purified Tregs (2×10^6) was injected intravenously 1 week later. Digital calipers were used to measure tumors regularly, and tumor volumes were calculated based on the formula length × width^2 × 0.52. A mixture of digestive solution with 0.5 mg/mL collagenase IV (Sigma) and 200 U/mL DNase I (Sigma) was used to purify tumor-infiltrating lymphocytes (TILs) from mangled tumor tissue.

Adoptive bone marrow transfer

A mixture of bone marrow (BM) from wild-type mice ($CD45.1^+CD45.2^+$) and *Tmed4*$^{\Delta Treg}$ ($CD45.1^-CD45.2^+$) was transplanted into 6-8 weeks old recipient mice ($CD45.1^+CD45.2^-$) removal of immune system through X-ray irradiation. Flow

cytometry analysis was conducted 8 weeks after transfer.

Induction and evaluation of EAE

To induce acute EAE, 10 to 12-week-old mice were injected subcutaneously in both flanks of back regions with 300 μg per mice of MOG_{35-55} peptide (Met-Glu-Val-Gly-Trp-Tyr-Arg-Ser-Pro-Phe-Ser-Arg-Val-Val-HisLeu-Tyr-Arg-Asn-Gly-Lys, Genemed Synthesis) in CFA (Incomplete Freund's adjuvant was purchased from IFA, Sigma) containing 5 mg/ml of heat-killed Mycobacterium tuberculosis H37Ra (BD Difco). Pertussis toxin (200 ng per mouse; List Biological Laboratories) was also administered to mice in PBS on the day of immunization and 48 hours later. Mice were examined daily for signs of EAE starting 1 week after immunization. The EAE disease symptoms were graded using the following standard method: 0: no abnormality; 1: tail paralysis; 2: mild hind limb weakness; 3: severe hind limb weakness; 4: complete hind limb paralysis; 5: quadriplegia or premature state or death. No group information is assigned when evaluating EAE scores.

Tissue processing and histology

Lung and spinal cords tissues dissected from *Tmed4*$^{f/f}$ and *Tmed4*$^{\Delta Treg}$ mice were fixed with 4% paraformaldehyde buffer overnight and washed with 70% ethanol the next day. After washing with 70% ethanol, the tissues were further processed by Wuhan Servicebio Technology Co., Ltd (paraffin-embedded, sectioned, and stained by hematoxylin&eosin and Luxol fast blue).

Flow cytometry

Single-cell suspension of lymphocytes were isolated from spleen, lymph nodes, lung, spinal cords, tumor, or lamina propria of mouse intestines (colon and small intestine). Live cells were selected after staining with Fixable Viability Stain (BD). To prepare CNS lymphocytes, the spinal cords and brains were ground on a cell strainer and washed with PBS. After centrifugation at 400g for 5 min, the cells were resuspended with 37% Percoll^{TM} (diluted with RPMI complete medium) to 10 ml. The cell suspension was then slowly and gently spread onto a 70% Percoll^{TM} density gradient at 20 °C, 2000 rpm and centrifuged for 20 min. CNS lymphocytes were isolated by collecting the interphase fraction between 30% and 70% Percoll^{TM}. After intensive washing in PBS, the cells were suspended in RPMI for further use. In FACS buffer (PBS + 2% FBS + 2 μM EDTA), cells were blocked by α-CD16/32 antibody (1:300) and stained with primary antibody (1:200) at 4 °C for 30 min. To detect intracellular cytokine production, IFN-γ, TNF-α and IL-17, using the fixation and permeablization kit (BD Biosciences) after cells were stimulated with stimulation cocktail (Invitrogen) for 12 hours. And for Foxp3 and ki67 staining, surface marker-stained cells were fixed, permeabilized using True Nuclear staining kit (Biolegend), and labeled with Foxp3-specific mAb (1:150). Flow cytometry data were acquired on LSRFortessa or LSRFortessa X20 (BD Biosciences) and analyzed with FlowJo_VX software (Tree Star).

Western blot

Cells were harvested after two washes with PBS and lysed in RIPA buffer on ice for 20 minutes to resolve proteins. Cell lysates were centrifuged at 13,000 rpm and 4°C for 10 minutes, and the protein concentrations were determined. A 10% SDS-PAGE is then used to resolve the proteins, and the membranes are electro-transferred to 0.45 μm PVDF (Immobilon-P) membranes. For blocking, 5% skim milk in 1 x TBS (10 mM Tris-Cl was added at pH 7.5 and 150 mM NaCl) was used and the membranes were left at room temperature for 20 mins. Afterwards, each primary antibody was probed overnight at 4°C on the membranes. A secondary antibody conjugated to HRP (CST) was used to detect membranes by enhanced chemiluminescence after three washes with 1 x TBS supplemented with 0.05% Tween-20. All primary antibodies were used at a 1:1000 dilution, with secondary HRP antibodies used at 1:10000 (diluted in 1% skim milk).

In vitro Treg suppression assay

The $CD4^+CD25^+$ Treg cells were purified from the spleens of 8-12-week-old *Tmed4*$^{f/f}$ and *Tmed4*$^{\Delta Treg}$ mice. The $CD4^+CD25^-$ T cells were purified from WT mice and labeled with e450 (eBioscience). $CD4^+CD25^-$ T cells with e450-labeled responder cells (1 x 10^5) and Treg cells (at ratios of 1:2, 1:1, 1:0.5) was co-cultured in 96-well plates coated with α-CD3 (1 μg/mL) and α-CD28 (1 μg/mL) for 3 days. In addition, in cases where Treg cells need to be pretreated before the Treg suppression assay, cells were stimulated with α-CD3/28 (1 μg/mL), IL-2 (200 U/mL) (Peprotech) in complete medium (containing 10% FBS and 1% penicillin and streptomycin) supplemented with drug for

time points as indicated.

In vitro cell treatments

For FOXP3 and IRE1α half-life test, cycloheximide (CHX, Selleck) was used at 1 μg/mL and 50 μg/mL on primary Treg cells or 293T cells for the indicated time points. For ER stress induction, primary Treg cells or 293T cells were pretreated with 1 μM thapsigargin (TG, Sigma-Aldrich) for 6-12 hours. 4μ8C, KIRA6 and GSK2656157 were purchased from Selleck and used at 10 μM in the inhibitory experiments. Acetylcysteine (N-acetylcysteine, NAC) and Sulforaphane were purchased from Selleck and used at 1mM and 10 uM respectively in the in vitro cell function rescuing experiments. For the Treg phenotype rescuing experiments in MC38 tumor model, the inoculated Treg cells were pretreated with NAC for 12 hours at 1 mM.

Q-PCR and RNA-seq

TRIzol reagent (Invitrogen) was used to extract total RNA of Treg cells purified from *Tmed4*$^{f/f}$ and *Tmed4*$^{\Delta Treg}$ mice and RNA was quantified with NanoDrop (ThermoFisher). The total RNA (1 μg) reverse transcribed using a reverse transcription kit (Yeasen). Gene-specific primers (SYBR Green, Yeasen) were used to quantify the indicated genes from purified cDNA. Gene expression levels in the same sample were normalized to β-actin or gapdh mRNA levels. Relative quantitation of target cDNA was determined by the formula $2^{\Delta CT}$, with ΔCT denoting fold increases above the set control value. The sequences of primers are listed in Supplemental Table 1. 1 μg total RNA was used for

RNAseq with three biological replicates per genotype and RNAseq was performed by Illumina with 150-base paired-end reads. A default alignment was performed using hisat2 with the mouse reference genome (mm10) as the reference. Genes with differential expression were identified and normalized by DESeq2 ($|\log2(\text{fold change})| \geq 1.5$; $p < 0.05$). R package Cluster Profiler was used to perform gene ontology (GO) and Kyoto Encyclopedia of Genes and Genomes pathway (KEGG) enrichment analyses, where the differentially expressed genes identified as described above were supplied as the input for genes by function and enrich GO and enrich KEGG, respectively. GSEA analysis was done by the software GSEA (version 4.1.0) available at https://www.gsea-msigdb.org/gsea/downloads.jsp. After loading expression data formats and phenotype data formats, we ran GSEA with default parameters.

Plasmid and transfections

TMED4 overexpressed human vector (TMED4 and TMED4-FLAG in pCDH-CMV-MCS-EF1-Puro) was generated by Azenta Life Sciences. BIP-HA (in pCDH or pCDNA3.0 vector), IRE1α-FLAG (pCDNA3.0) and HRD1-HA (pCDNA3.0) overexpressed human plasmids were generously provided by Dr. Zhaoyuan Hou at Shanghai Jiao Tong University School of Medicine. IRE1α overexpressed human plasmid was bountifully provided by Dr. Bin Li at Shanghai Jiao Tong University School of Medicine. One 6-well plate containing 2-3 x 10^6 293T cells was transfected with 1 μg of plasmids each and PEI. After 24-48 hours cells were either or not treated with fresh media with 1 μM thapsigargin for 5 h and followed cell lysis process for

further use.

siRNA knockdown

iTreg cells were transfected by electroporation as described previously with 50 nM mouse PERK or nontargeting control siRNA. Electroporation was carried out using the Mouse T cell Nucleofector Kit (Lonza), Transfected cells were lysed 48–72 h after transfection for further experiment. The sequences specific for PERK are shown in Supplemental Table 2.

Seahorse assays

Treg cells were stimulated for 24 hours with α-CD3/28 antibodies and attached to culture plates with CellTak (Corning) at a density of 3 x 10^5 per well. Oxygen consumption rate (OCR) and extracellular acidification rate (ECAR) of T cells were measured on the Seahorse Biosciences XF96 Extracellular Flux Analyzer (Seahorse Biosciences), following are the concentrations of compounds injected: 10 mM glucose, 100 μM oligomycin, 100 μM FCCP, 50 μM rotenone/antimycin A (Agilent Technologies).

T cell transfer colitis model

Rag1-deficient mice are injected with naïve $CD4^+CD25^-CD45RB^{hi}$ splenic T cells (0.3 million cells/mouse) isolated from B6.SJL ($CD45.1^+$) mice alone or combination $CD4^+CD25^+$ Treg cells from $Tmed4^{f/f}$ or $Tmed4^{\Delta Treg}$ ($CD45.2^+$) mice (0.1 million

cells/mouse). Mice were monitored weekly for weight loss for 6 weeks, after which mice were sacrificed for further analysis.

iTreg cell virus infection model

Naïve $CD4^+$ were sorted from *Tmed4*$^{f/f}$ or *Tmed4*$^{\Delta Treg}$ and induced into iTreg as described before. The Sindbis expression system were provided by Dr. Peng Zhang (Shanghai Jiao Tong University School of Medicine). iTreg cells were infected with GFP-control or IRE1α-GFP Sindbis concentrated virus with 5 μg/ml polybrene at 900g, 32 °C for 2 h, and the fresh induction differentiation medium was replaced after 6 hours. After 24 hours, the GFP^+ cells were sorted for following experiments.

Statistics

A Pearson's correlation coefficient was used to analyze the correlation between genes in the human data shown in Supplemental Figure 1 and 6. Statistical analyses are presented using two-tailed Student's t tests or one-way ANOVA with Tukey's multiple-comparison test. Data were shown as mean ± SEM. Statistical analysis was performed with GraphPad PRISM software 7.0 (GraphPad Inc., La Jolla, CA, USA). A p value of less than 0.05 was considered statistically significant.

Study approval

Each colon adenocarcinoma or stomach adenocarcinoma patient provided informed consent prior to inclusion in the study, and all procedures were approved by the Ethics Committee of Ruijin Hospital at SJTU-SM (2019-186). All mouse experimental

procedures were conducted with the approval of the Department of Laboratory Animal Science (DLAS), SJTU-SM.

DATA AVAILABILITY

Lead contact

Further information and requests for resources and reagents should be directed to and will be fulfilled by the lead contact, Xuefeng Wu (xuefengwu@shsmu.edu.cn).

Materials availability

This study did not generate new unique reagents.

Data and code availability

RNA-seq data is provided via the Sequence Read Archive (SRA), accession number PRJNA1025114. This paper does not report original code. All other data are reported in the Supporting Data Values file. Any additional information required to reanalyze the data reported in this paper is available from the lead contact upon request.

AUTHOR CONTRIBUTIONS

ZJ and HW designed and performed the experiments, prepared the figures, and wrote the manuscript; Xiaoxia Wang designed experiments and helped to analyze data; HD analyzed TCGA database; YT, J. Li, XL, J. Liu, JN, EJW, HX, CG, and Xinyu Wang contributed to part of the experiments; KZ, PZ helped with Sindbis experiments; ZH,

YL, and ZW provided technical support, discussion, and advice; BS, Bo Li, YH and Bin Li supervised the research; X. Wu designed experiments, supervised the research, and wrote the manuscript.

ACKNOWLEDGMENTS

This work was supported by the National Key Research and Development Program of China Grant 2021YFC2701800, National Natural Science Foundation of China Grants 31670910 and 82170748), Science and Technology Innovation Plan of Shanghai Science and Technology Commission Grants (21ZR1456200 and 23ZR1455400), Innovative Research Team of High-Level Local Universities in Shanghai Grant SHSMUZDCX20212000, Shanghai Municipal Health Commission (202040119), and by Shanghai Frontiers Science Center of Cellular Homeostasis Regulation and Human Diseases.

DECLARATION OF INTERESTS

The authors declare no competing interests.

FIGURES WITH TITLES AND LEGENDS

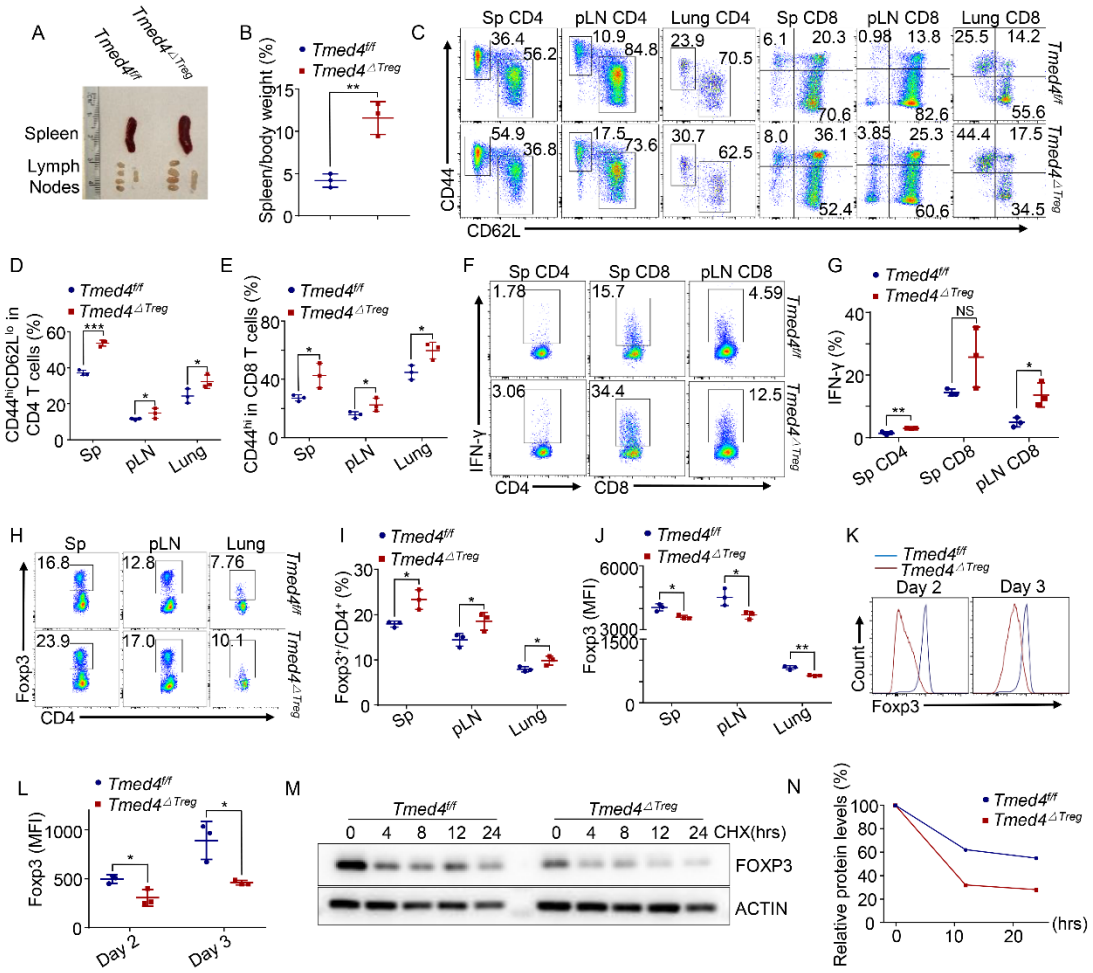

Figure 1. Treg cell specific *Tmed4* knockout (*Tmed4*$^{\Delta Treg}$) mice exhibit T cell hyper-activation, and impaired Foxp3 stability in Treg cells.

(A) Images of spleen and peripheral lymph nodes (pLNs) of 12-week-old gender matched littermate *Tmed4*$^{f/f}$ (WT) mice and *Tmed4*$^{\Delta Treg}$ (cKO) mice.

(B) Speen/Body weight ratios of *Tmed4*$^{f/f}$ and *Tmed4*$^{\Delta Treg}$ mice (n = 3).

(C-E) Flow cytometry (FCM) plots (C) and analysis (D and E) of effector CD4^{+} and CD8^{+} T cells isolated from spleen, pLNs and lungs of *Tmed4*$^{f/f}$ and *Tmed4*$^{\Delta Treg}$ mice (n = 3).

(F and G) FCM plots (F) and analysis (G) of IFN-γ-producing $CD4^+$ and $CD8^+$ T cells from spleen and pLN of *Tmed4*$^{f/f}$ and *Tmed4*$^{\Delta Treg}$ mice (n = 3).

(H and I) FCM plots (H) and analysis (I) of Treg cell frequencies in $CD4^+$ T cells from spleen, pLNs and lungs of *Tmed4*$^{f/f}$ and *Tmed4*$^{\Delta Treg}$ mice (n = 3).

(J) FCM analysis of mean fluorescence intensity (MFI) of Foxp3 in Treg cells from spleen, pLNs and lungs of *Tmed4*$^{f/f}$ and *Tmed4*$^{\Delta Treg}$ mice (n = 3).

(K and L) FCM levels (K) and analysis (L) of Foxp3 MFI of iTreg cells ($CD4^+CD25^+Foxp3^+$) inducted in vitro 2 or 3 days after the naïve T cells were purified and cultured with differentiation inducers (n = 3).

(M and N) Western blotting (M) and quantitative analysis (N) of FOXP3 decay in WT and *Tmed4*-deficient Treg cells purified from spleen and pLNs treated with 1 μg/ml of cycloheximide (CHX) for the indicated time courses.

Data are presented as mean ± SEM of biologically independent samples and represents at least 3 independent experiments, each involving 3 mice per group. NS, not significant, *p < 0.05, **p < 0.01, ***p < 0.001, and ****p < 0.0001, by two-tailed Student's t test.

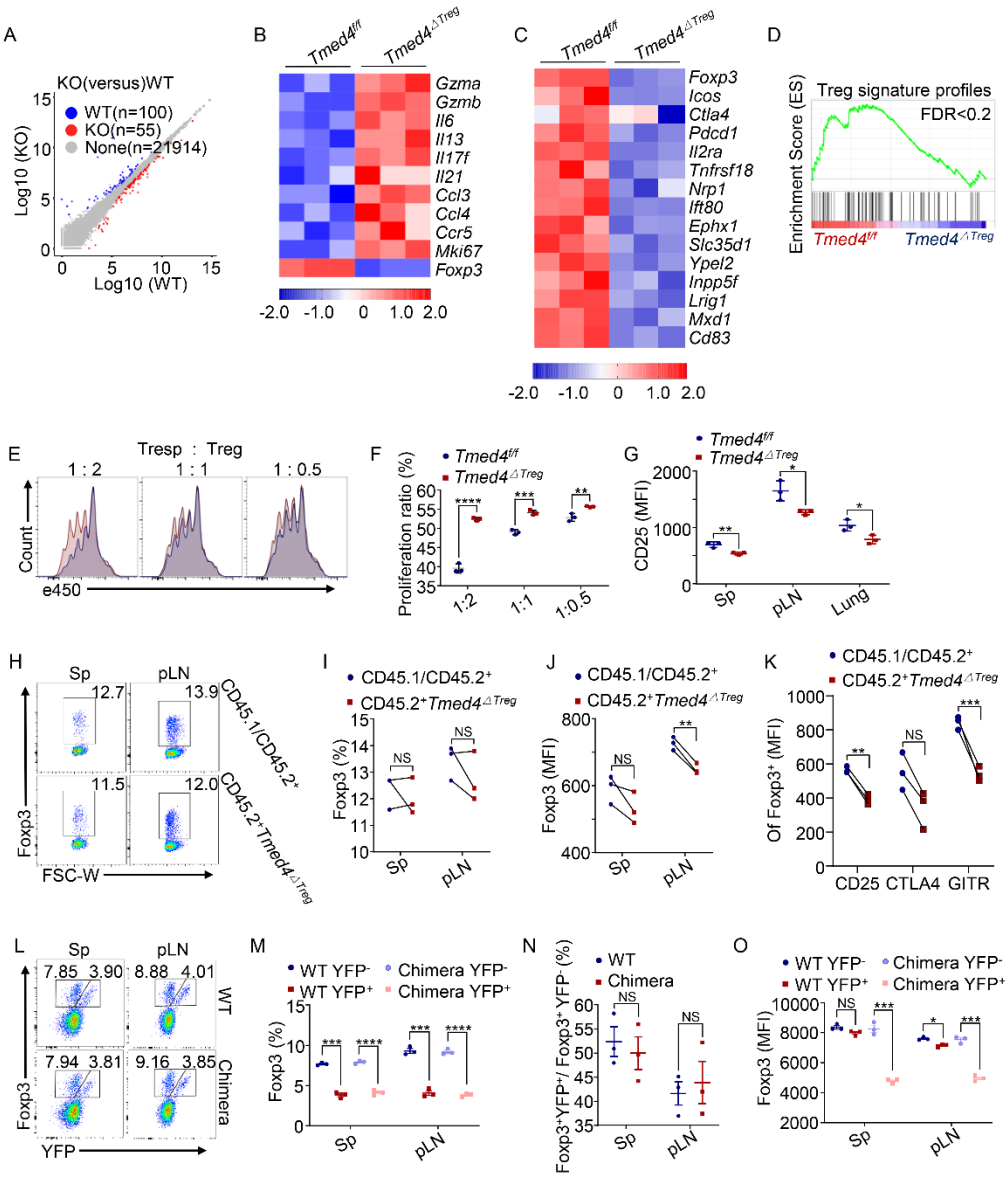

Figure 2. TMED4 deficiency alters Treg cells' signature profiles in a cell intrinsic manner.

(A) Scatterplot showing global gene expression profiles of Treg cells from *Tmed4*$^{f/f}$ and *Tmed4*$^{\Delta Treg}$ mice stimulated with α-CD3/28. Transcripts with a |log2 (fold change) | > 0.5 and p < 0.05 in *Tmed4*-deficient Treg cells are shown in blue or red.

(B and C) Heatmaps of gene clusters of differentially expressed genes (DEGs) of effector-like (B) genes and Treg signature profiles (C) and between WT and *Tmed4*-

deficient Treg cells. Red and blue represent relatively higher and lower levels of expression of indicated genes, respectively. The colors indicate the value of log2 fold change (n = 3).

(D) GSEA plots showing the enrichment of 'Treg signature profiles' (FDR < 0.2) gene set.

(E and F) FCM levels (E) and statistical analysis (F) of in vitro suppressive assay of Treg cells purified from spleen of *Tmed4*$^{f/f}$ and *Tmed4*$^{\Delta Treg}$ mice, assessed by proliferation of activated CD4$^+$ T cells in the presence of various ratios (Tresp: Treg = 1:2, 1:1 and 1:0.5) of Treg cells (n = 3, detected on day 3).

(G) FCM analysis of mean fluorescence intensity (MFI) of CD25 in Treg cells from spleen, pLNs and lungs of *Tmed4*$^{f/f}$ and *Tmed4*$^{\Delta Treg}$ mice (n = 3).

(H and I) Flow cytometry (FCM) plots (H) and analysis (I) of frequencies of Foxp3$^+$ Treg cell in bone marrow (BM) chimeric mice (n = 3).

(J and K) FCM analysis of Foxp3 (J), CD25, CTLA4 and GITR MFI (K) from spleen and pLN in bone marrow (BM) chimeric mice (n = 3).

(L and M) FCM plots (L) and Foxp3 frequencies (M) of both YFP$^+$ and YFP$^-$ Treg cells in spleen and pLN of female WT and chimera mice (n = 3).

(N) The ratio of YFP$^+$ to YFP$^-$ Treg cells in spleen and pLN within female WT or chimera mice (n = 3).

(O) FCM analysis of Foxp3 MFI between YFP$^+$ and YFP$^-$ Treg cells in female WT and chimera mice (n = 3).

Data are presented as mean ± SEM of biologically independent samples and represents at least 3 independent experiments, each involving 3 mice per group. NS, not significant, *$p < 0.05$, **$p < 0.01$, ***$p < 0.001$, and ****$p < 0.0001$, by two-tailed Student's t test.

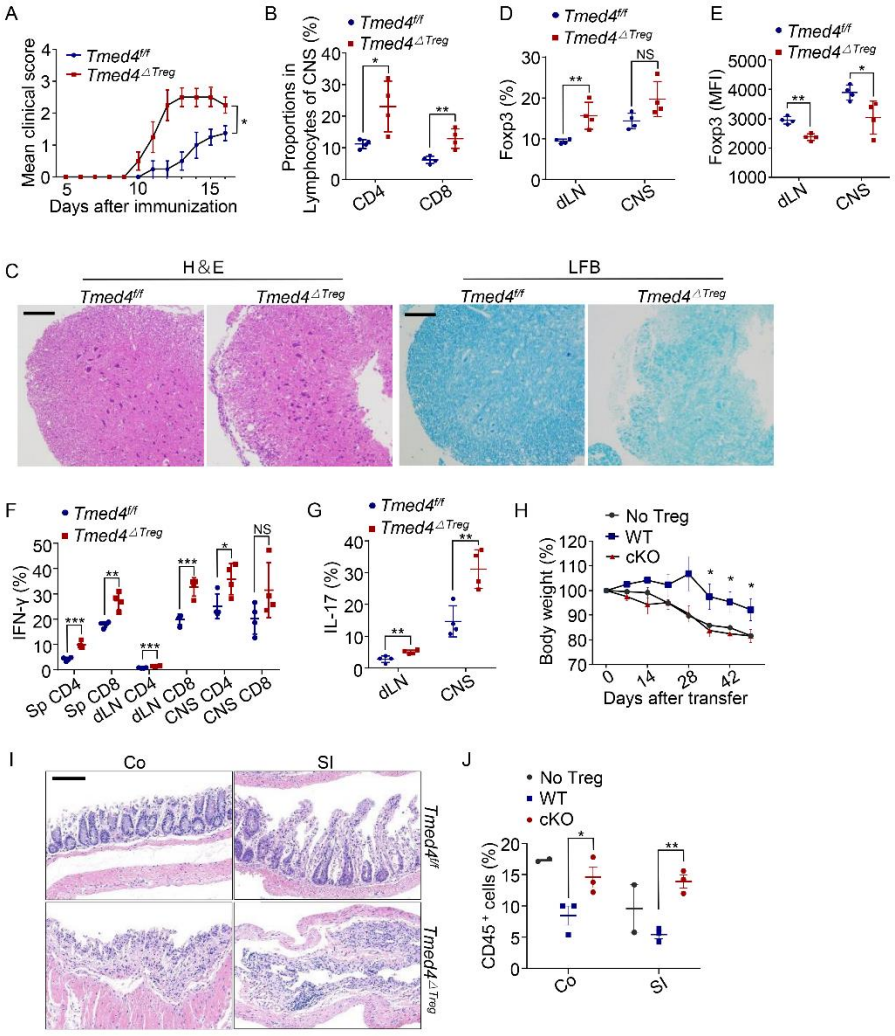

Figure 3. Loss of *Tmed4* in Treg cells leads to more exacerbated inflammatory phenotype in mice.

(A) Mean clinical score of diseased *Tmed4*$^{f/f}$ and *Tmed4*$^{\Delta Treg}$ mice (n = 4).

(B) FCM analysis of CD4^{+} and CD8^{+} T cell proportions isolated from the CNS (central nervous system) of diseased *Tmed4*$^{f/f}$ and *Tmed4*$^{\Delta Treg}$ mice 16 days after disease induction (n = 4).

(C) Haematoxylin and eosin (H&E) and Luxol Fast Blue (LFB) staining of spinal cord sections from diseased *Tmed4*$^{f/f}$ and *Tmed4*$^{\Delta Treg}$ mice (16 days after

immunization). Scale bars: 100 μm. Samples are selected from one *Tmed4*$^{f/f}$ (clinical score: 1) and one *Tmed4*$^{\Delta Treg}$ (clinical score: 3) mouse.

(D and E) FCM analysis of Treg frequencies (D) and Foxp3 MFI (E) from dLNs and CNS (n = 4).

(F and G) FCM analysis of IFN-γ-producing (F) $CD4^+$ and $CD8^+$ T cells from spleen, dLNs and CNS, and IL-17-producing (G) $CD4^+$ T cells from dLNs and CNS in diseased *Tmed4*$^{f/f}$ and *Tmed4*$^{\Delta Treg}$ mice (n = 4).

(H) The curve of body weight loss percentage. Injections of $CD4^+CD45RB^{hi}CD25^{lo}$ naïve T cells were made in $Rag1^{-/-}$ mice alone or in combination with Treg cells isolated from *Tmed4*$^{f/f}$ and *Tmed4*$^{\Delta Treg}$ mice. The body weight is presented relative to the initial weight in each case (n = 3 for mice co-injected with naïve T mixed *Tmed4*$^{f/f}$ or *Tmed4*$^{\Delta Treg}$ Treg cells respectively, n = 2 for mice injected with naïve T cells alone).

(I) H&E staining of colon (Co) and the small intestine (SI) after adoptive transfer. Scale bars: 100 μm.

(J) Percentages of $CD45^+$ cells infiltrating into colon and small intestine (n = 3 for mice co-injected with naïve T mixed WT or *Tmed4*-deficient Treg cells respectively, n = 2 for mice injected with naïve T cells alone).

Data are presented as mean ± SEM of biologically independent samples and each represents 3 independent experiments, each involving 2-4 mice per group. NS, not significant, *$p < 0.05$, **$p < 0.01$, ***$p < 0.001$, and ****$p < 0.0001$, by two-way analysis of ANOVA (A), one-way analysis of ANOVA with Tukey's multiple-comparison test (H) and two-tailed Student's t test for other analysis.

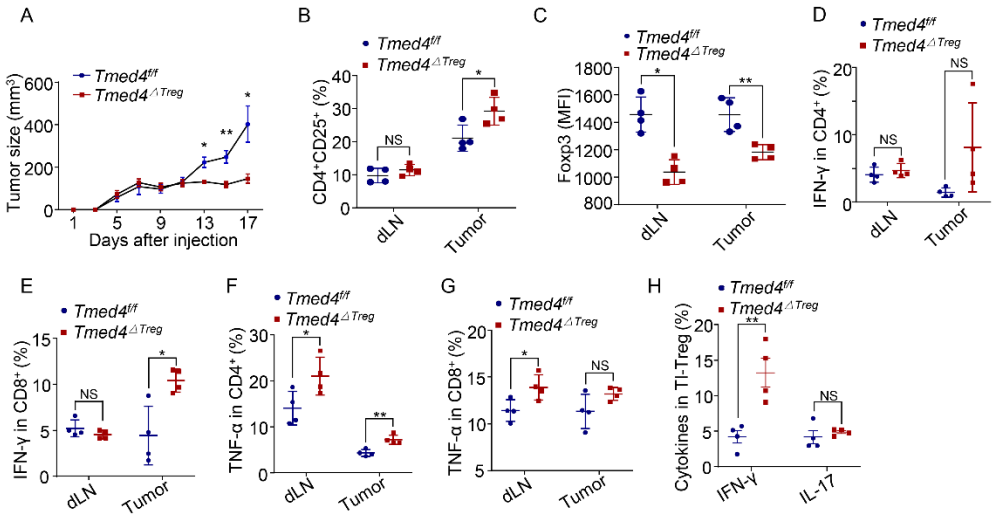

Figure 4. Loss of *Tmed4* in Treg cells leads boosted anti-tumor immunity in mice.

(A) Growth curves of tumors derived from subcutaneously (s.c.) inoculated MC38 cells in *Tmed4*$^{f/f}$ and *Tmed4*$^{\Delta Treg}$ mice (n = 4).

(B and C) FCM analysis of $CD4^+CD25^+$ frequencies (B) and Foxp3 MFI (C) of dLNs and tumor infiltrating $CD4^+Foxp3^+$ Treg cells of tumor bearing *Tmed4*$^{f/f}$ and *Tmed4*$^{\Delta Treg}$ mice (n = 4).

(D-G) FCM analysis of percentages of IFN-γ (D and E) and TNF-α (F and G) secreting in tumor infiltrating $CD4^+$ and $CD8^+$ T cells from dLNs and tumors from tumor bearing *Tmed4*$^{f/f}$ and *Tmed4*$^{\Delta Treg}$ mice (n = 4).

(H) Percentages of tumor infiltrating Treg cells that producing IFN-γ and IL-17 from tumor bearing $Tmed4^{f/f}$ and $Tmed4^{\Delta Treg}$ mice (n = 4).

Data are presented as mean ± SEM of biologically independent samples and each represents 3 independent experiments, each involving 2-4 mice per group. NS, not significant, *p < 0.05, **p < 0.01, ***p < 0.001, and ****p < 0.0001, by two-tailed Student's t test

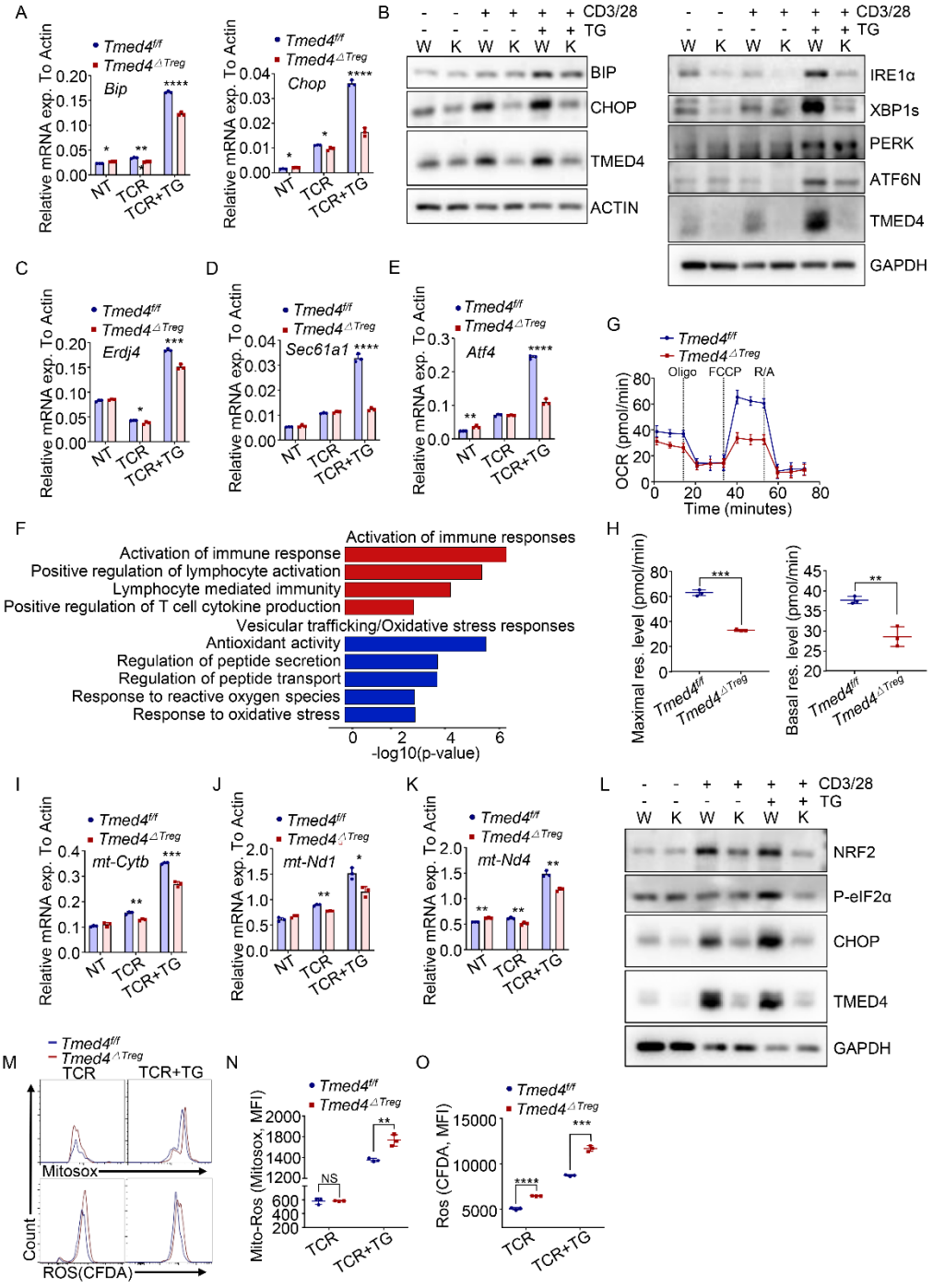

Figure 5. *Tmed4*-deficiency leads to impaired ER stress response, mitochondria integrity and accumulated ROS in Treg cells.

(A) Relative mRNA expression of *Bip* and *Chop* in WT and *Tmed4*-deficient Treg cells under resting or with α-CD3/28 (TCR) alone or together with 1 μM thapsigargin (TG) to induce ER stress for 16-20 h (n = 3).

(B) WB analysis of the ER stress-related regulator proteins and their downstream molecules in WT and *Tmed4*-deficient Treg cells treated with DMSO, α-CD3/28 only or together with 1 μM thapsigargin (TG) for 16-20 h.

(C-E) Relative mRNA expression of *Erdj4* (C), *Sec61a1* (D) and *Atf4* (E) in WT and *Tmed4*-deficient Treg cells under resting or with α-CD3/28 (TCR) alone or together with 1 μM thapsigargin (TG) to induce ER stress for 16-20 h (n = 3).

(F) KEGG and GO pathways enrichment analysis of *Tmed4*-deficient Treg cells compared to WT Treg cells. Selected Up-regulated (red bars) and down-regulated (blue bars) pathways are shown in *Tmed4*-deficient Treg cells.

(G and H) The curve (G) and quantitative analysis (H) of oxygen consumption rate (OCR) of WT and *Tmed4*-deficient Treg cells stimulated with α-CD3/28 for 16-20 h (n = 3).

(I-K) Relative mRNA expression of *mt-Cytb* (I), *mt-Nd1* (J) and *mt-Nd4* (K) in WT and *Tmed4*-deficient Treg cells under resting or with α-CD3/28 (TCR) or together with 1 μM thapsigargin (TG) stimulation for 16-20 h (n = 3).

(L) WB analysis of the PERK pathway-related proteins in WT and *Tmed4*-deficient Treg cells treated with α-CD3/28 only or together with 1 μM thapsigargin (TG) for 16-20 h.

(M-O) Levels of mitochondrial ROS (M, upper lane) and cellular total ROS (M, lower lane) stained Mito-SOX and CFDA (H2DCFDA), respectively, and quantitative analysis of their MFI (N and O) in WT and *Tmed4*-deficient splenic Treg cells

stimulated with α-CD3/28 (TCR) alone or together with 1 μM thapsigargin (TG) for 16-20 h (n = 3).

Data are presented as mean ± SEM of biologically independent samples and each represents at least 3 independent experiments, each involving 3 mice per group. NS, not significant, *p < 0.05, **p < 0.01, ***p < 0.001, and ****p < 0.0001, by two-tailed Student's t test.

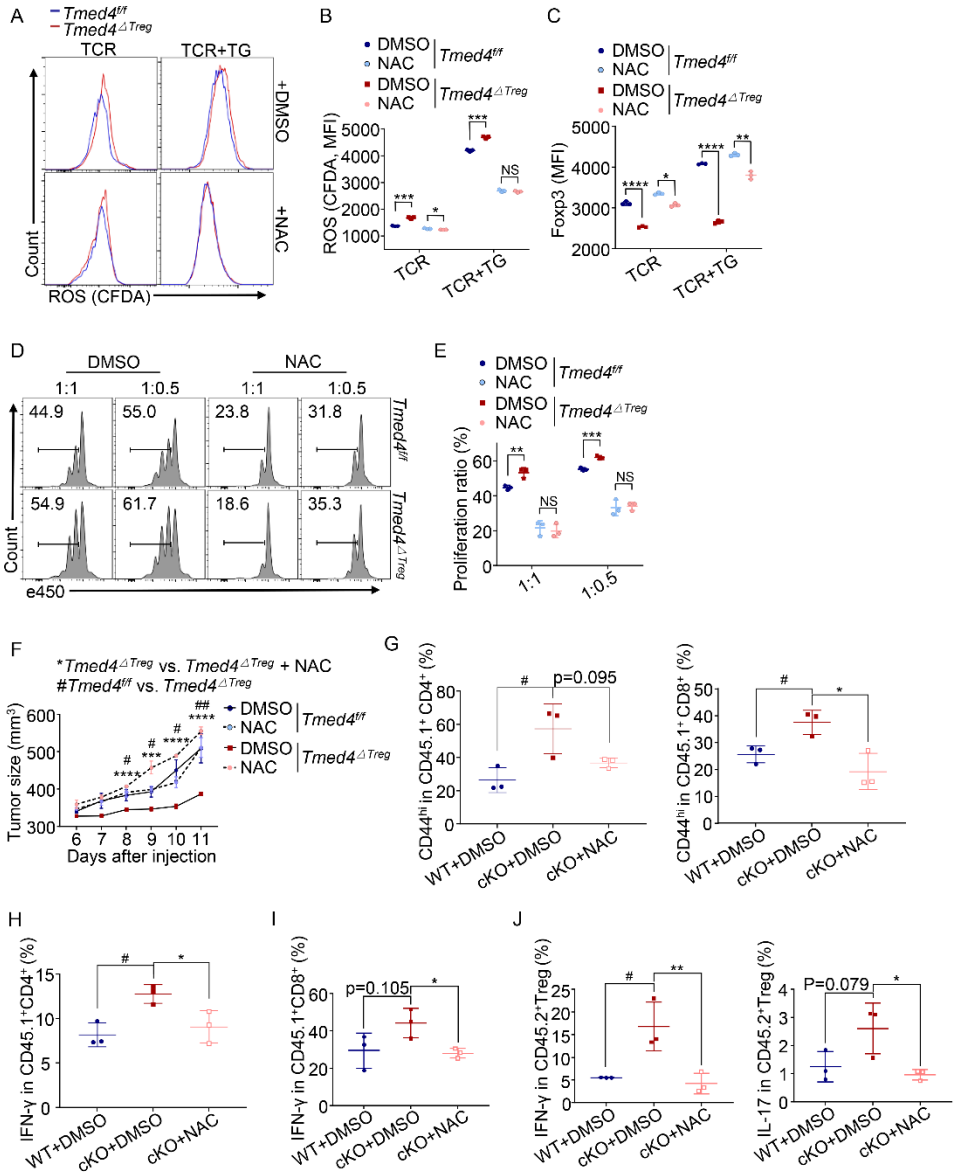

Figure 6. ROS scavenger or NRF2 inducer restores Foxp3 expression and suppressive function of *Tmed4*-deficient Treg cells.

(A-C) The total cellular ROS levels (A) of splenic Treg cells stimulated with TCR alone or together with 1 μM thapsigargin (TG) for 12 h in the presence or absence of NAC (N-acetylcysteine), and their quantitative analysis on MFI of ROS (B) and Foxp3 (C) expressions (n = 3).

(D and E) FCM levels (D) and statistical analysis (E) of in vitro suppressive assay of Treg cells purified from spleen and lymph nodes of *Tmed4*$^{f/f}$ and *Tmed4*$^{\Delta Treg}$ mice,

assessed by proliferation of activated $CD4^+$ T cells in the presence of indicated ratios of Treg cells pretreated with DMSO or NAC for 12 h. (n = 3, detected on day 3)

(F) Tumor growth curves of $CD45.1^+$ mice injected (s.c.) with MC38 cells together with WT or *Tmed4*-deficient Treg cells. Both types of Treg cells pretreated with α-CD3/28 for 12 h in the presence or absence of NAC and then intravenously (i.v.) on day 0 and day 7 (n = 4).

(G) FCM analysis of proportions of activated host $CD45.1^+CD4^+$ (G, left) and $CD45.1^+CD8^+$ (G, right) T cells of WT and KO groups in the presence and absence of NAC respectively. (n = 3).

(H and I) IFN-γ-producing host $CD45.1^+CD4^+$ (H) and $CD45.1^+CD8^+$ (I) T cells of WT and KO groups in the presence and absence of NAC respectively (n = 3).

(J) IFN-γ (J, left) and IL-17 (J, right)-producing donor $CD45.2^+$ Treg cells of WT and KO groups in the presence and absence of NAC respectively (n = 3).

Data are presented as mean ± SEM of biologically independent samples. Tumor rescuing model represents 2 independent experiments and others represent 3 independent experiments, each involving 3-4 mice per group. NS, not significant, *p < 0.05 or #p < 0.05, **p < 0.01 or ##p < 0.01, ***p < 0.001, and ****p < 0.0001, by one-way analysis of ANOVA with Tukey's multiple-comparison test (F-J) and two-tailed Student's t test.

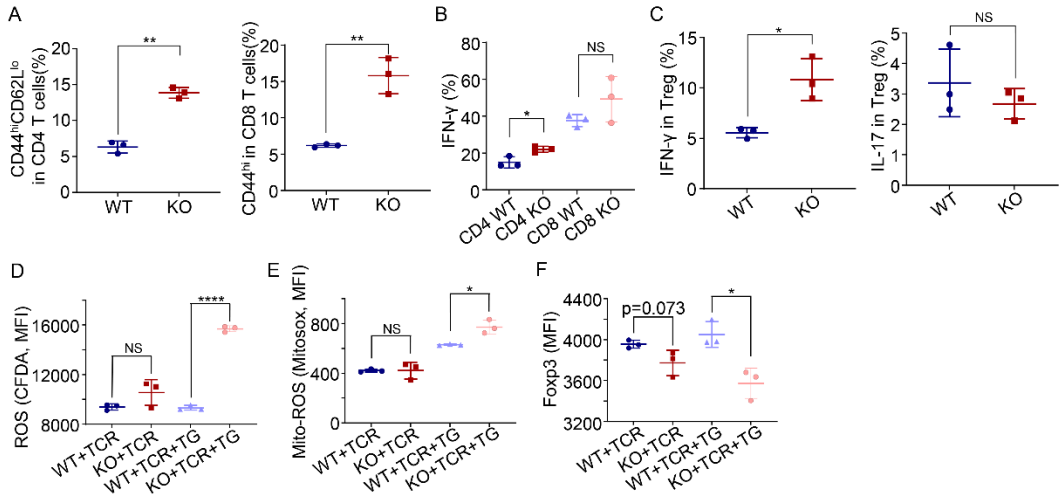

Figure 7. Treg cell specific *Ern1* knockout (*Ern1*$^{\Delta Treg}$) phenocopied *Tmed4*$^{\Delta Treg}$ mice.

(A and B) The statistical analysis of the proportions of activation (A) and IFN-γ-producing (B) CD4^{+} and CD8^{+} T cells from spleens of *Ern1*$^{f/f}$ and *Ern1*$^{\Delta Treg}$ mice (n = 3).

(C) The statistical analysis of IFN-γ (C, left) and IL-17 (C, right)-producing Treg cells from spleens of *Ern1*$^{f/f}$ and *Ern1*$^{\Delta Treg}$ mice (n = 3).

(D-F) Quantitative analysis of the MFI of total ROS (D), mitochondrial ROS (E) and Foxp3 (F) in splenic Treg cells from *Ern1*$^{f/f}$ and *Ern1*$^{\Delta Treg}$ mice, treated with α-CD3/28 (TCR) alone or together with 1 μM thapsigargin (TG) for 16-20 h (n = 3).

Data are presented as mean ± SEM of biologically independent samples and each represents at least 3 independent experiments, each involving 3 mice per group. NS, not significant, *p < 0.05, **p < 0.01, ***p < 0.001, and ****p < 0.0001, by one-way analysis of ANOVA with Tukey's multiple-comparison test (D-F) and two-tailed Student's t test.

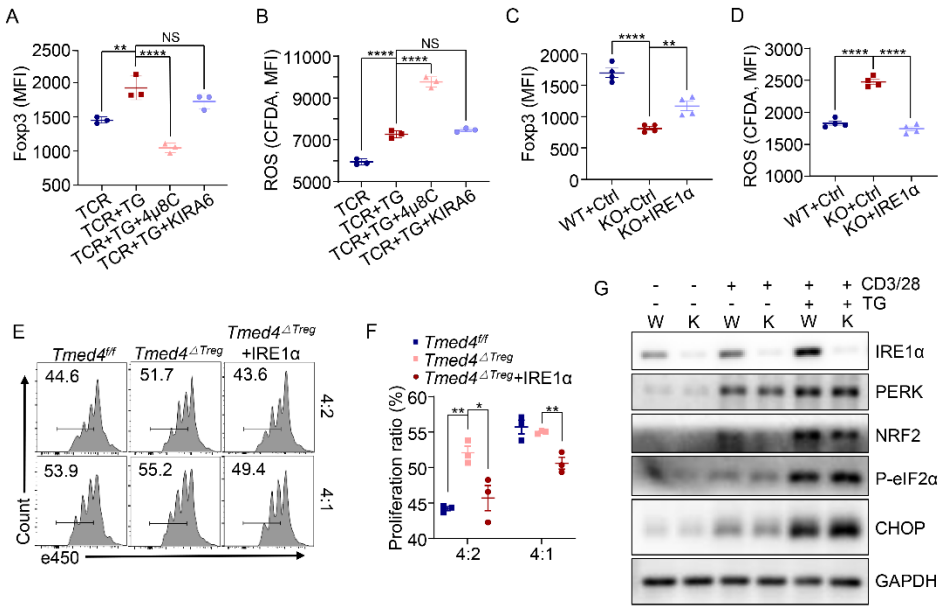

Figure 8. *Tmed4*-deficiency in Treg cells leads to lower Foxp3 expression and ROS accumulation in an IRE1α-XBP1 axis dependent manner.

(A and B) Expression levels of Foxp3 (A) and cellular ROS (B) of WT splenic Treg cells treated with α-CD3/28 (TCR) with 1 μM thapsigargin (TG) and IRE1α inhibitors 4μ8C or KIRA6 for 16-20 h (n = 3).

(C and D) Quantitative analysis of the MFI of Foxp3 expression (C) and ROS (D) in WT and *Tmed4*-deficient splenic Treg cells without (Ctrl) or with forcible IRE1α expression. Cells were treated with 1 μM thapsigargin (TG) for 16-20 h (n = 3).

(E and F) FCM levels (E) and statistical analysis (F) of in vitro suppressive assay of Treg cells purified from spleens of $Tmed4^{f/f}$, $Tmed4^{\Delta Treg}$ mice or $Tmed4^{\Delta Treg}$ Treg cells with IRE1α-forcible expression ($Tmed4^{\Delta Treg}$ +IRE1α), and assessed by proliferation of activated $CD4^+$ T cells at various ratios (Tresp : Treg = 4:2 and 4:1) of Treg cells (n = 3, detected on day 3).

(G) WB analysis of the PERK and its downstream proteins in *Ern1*$^{f/f}$ (W) and *Ern1*$^{\Delta Treg}$ (K) Treg cells treated with DMSO, α-CD3/28 only or together with 1 μM thapsigargin (TG) for 16-20 h.

Data are presented as mean ± SEM of biologically independent samples and each represents at least 3 independent experiments, each involving 3 mice per group. NS, not significant, *$p < 0.05$, **$p < 0.01$, ***$p < 0.001$, and ****$p < 0.0001$, by one-way analysis of ANOVA with Tukey's multiple-comparison test (A-D, and F).

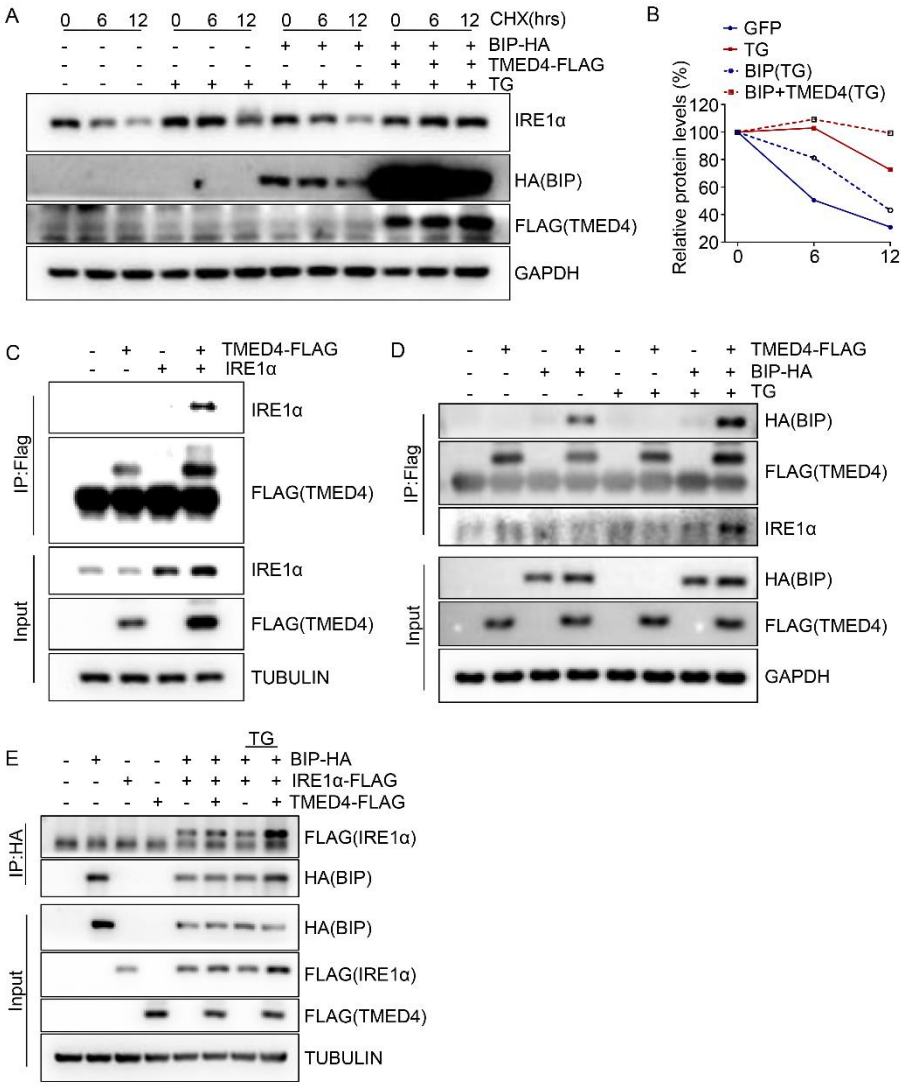

Figure 9. TMED4 suppresses IRE1α degradation in collaboration with BIP.

(A and B) WB (A) and quantitative analysis (B) of IRE1α decay in HEK293T cells transfected with or without TMED4-FLAG and BIP-HA under the treatment of 50 μg/ml of CHX with or without 1 μM thapsigargin (TG) for the indicated times lengths.

(C and D) WB analysis of immunoprecipitation assays on HEK293T cells transfected with TMED4-FLAG and IRE1α (C), or BIP-HA (D) which were either not or treated with 1 μM thapsigargin (TG) for 6 h.

(E) WB analysis of immunoprecipitation assays on HEK293T cells transfected with BIP-HA, IRE1α-FLAG or TMED4-FLAG which were either not or treated with thapsigargin (TG) for 6 h as indicated.

Each represents 3 independent experiments with similar results.

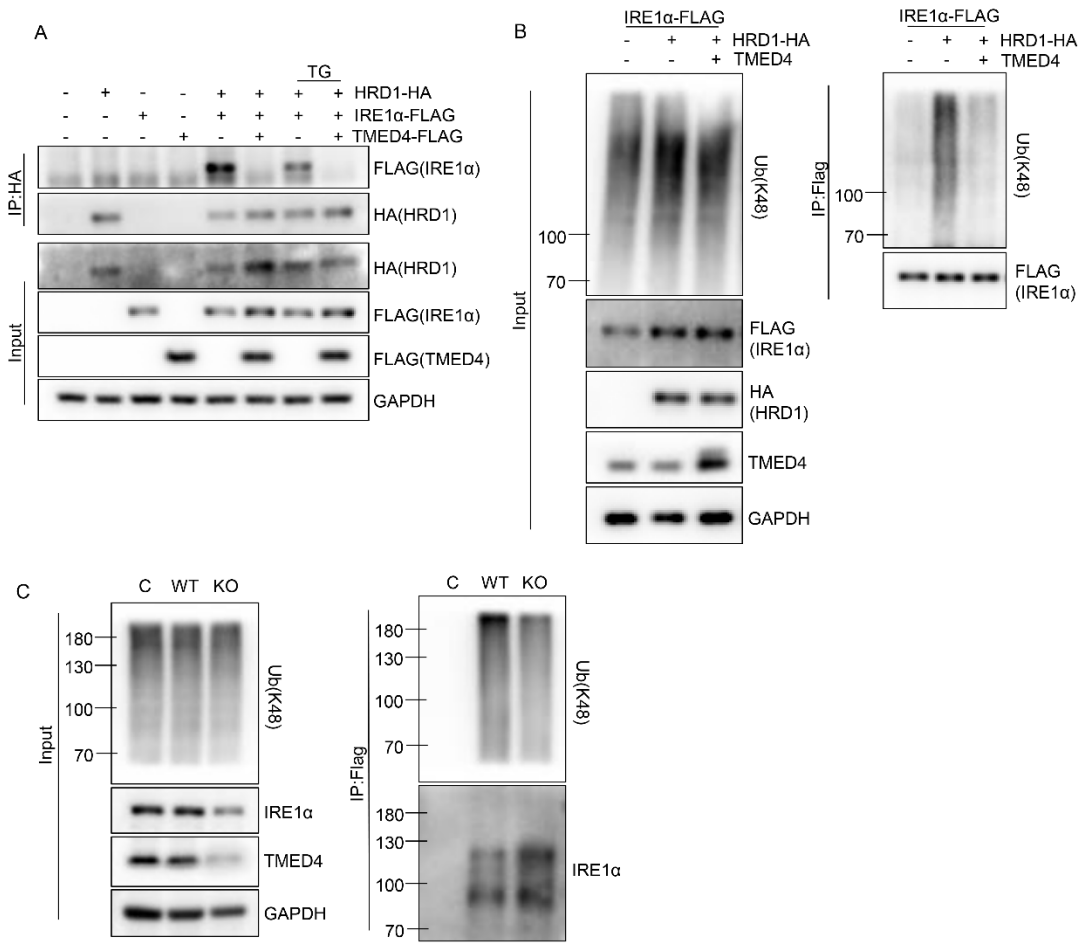

Figure 10. TMED4 suppresses HRD1/BIP-mediated IRE1α degradation.

(A) WB analysis of immunoprecipitation assays on HEK293T cells transfected with indicated plasmids which were either not or treated with thapsigargin (TG) for 6 h as indicated.

(B) WB analysis of IRE1α K48-linked polyubiquitination assays on HEK293T cells transfected with indicated plasmids.

(C) WB analysis of IRE1α K48-linked polyubiquitination assay on primary WT and *Tmed4*-deficient iTreg cells using anti-K48-linked Ub-FLAG beads.

Each represents 3 independent experiments with similar results.

REFERENCES

1. Sakaguchi S, Yamaguchi T, Nomura T, and Ono M. Regulatory T cells and immune tolerance. *Cell.* 2008;133(5):775-87.
2. Josefowicz SZ, Lu LF, and Rudensky AY. Regulatory T cells: mechanisms of differentiation and function. *Annu Rev Immunol.* 2012;30:531-64.
3. Rudensky A. Foxp3 and dominant tolerance. *Philos Trans R Soc Lond B Biol Sci.* 2005;360(1461):1645-6.
4. Wan YY, and Flavell RA. Regulatory T-cell functions are subverted and converted owing to attenuated Foxp3 expression. *Nature.* 2007;445(7129):766-70.
5. Fontenot JD, Rasmussen JP, Williams LM, Dooley JL, Farr AG, and Rudensky AY. Regulatory T cell lineage specification by the forkhead transcription factor foxp3. *Immunity.* 2005;22(3):329-41.
6. Martinon F, Chen X, Lee AH, and Glimcher LH. TLR activation of the transcription factor XBP1 regulates innate immune responses in macrophages. *Nat Immunol.* 2010;11(5):411-8.
7. Qiu Q, Zheng Z, Chang L, Zhao YS, Tan C, Dandekar A, et al. Toll-like receptor-mediated IRE1alpha activation as a therapeutic target for inflammatory arthritis. *EMBO J.* 2013;32(18):2477-90.
8. Xu Y, Melo-Cardenas J, Zhang Y, Gau I, Wei J, Montauti E, et al. The E3 ligase Hrd1 stabilizes Tregs by antagonizing inflammatory cytokine-induced ER stress response. *JCI Insight.* 2019;4(5).
9. Guerriero CJ, and Brodsky JL. The delicate balance between secreted protein folding and endoplasmic reticulum-associated degradation in human physiology. *Physiol Rev.* 2012;92(2):537-76.
10. Olzmann JA, Kopito RR, and Christianson JC. The mammalian endoplasmic reticulum-associated degradation system. *Cold Spring Harb Perspect Biol.* 2013;5(9).
11. Hetz C, Zhang K, and Kaufman RJ. Mechanisms, regulation and functions of the unfolded protein response. *Nat Rev Mol Cell Biol.* 2020;21(8):421-38.
12. Sun S, Shi G, Sha H, Ji Y, Han X, Shu X, et al. IRE1alpha is an endogenous substrate of endoplasmic-reticulum-associated degradation. *Nat Cell Biol.* 2015;17(12):1546-55.
13. Solanki NR, Stadanlick JE, Zhang Y, Duc AC, Lee SY, Lauritsen JP, et al. Rpl22 Loss Selectively Impairs alphabeta T Cell Development by Dysregulating Endoplasmic Reticulum Stress Signaling. *J Immunol.* 2016;197(6):2280-9.
14. Pino SC, O'Sullivan-Murphy B, Lidstone EA, Thornley TB, Jurczyk A, Urano F, et al. Protein kinase C signaling during T cell activation induces the endoplasmic reticulum stress response. *Cell Stress Chaperones.* 2008;13(4):421-34.
15. Kemp KL, Lin Z, Zhao F, Gao B, Song J, Zhang K, et al. The serine-threonine kinase inositol-requiring enzyme 1alpha (IRE1alpha) promotes IL-4 production in T helper cells. *J Biol Chem.* 2013;288(46):33272-82.

16. Thaxton JE, Wallace C, Riesenberg B, Zhang Y, Paulos CM, Beeson CC, et al. Modulation of Endoplasmic Reticulum Stress Controls CD4(+) T-cell Activation and Antitumor Function. *Cancer Immunol Res.* 2017;5(8):666-75.
17. Song M, Sandoval TA, Chae CS, Chopra S, Tan C, Rutkowski MR, et al. IRE1alpha-XBP1 controls T cell function in ovarian cancer by regulating mitochondrial activity. *Nature.* 2018;562(7727):423-8.
18. Zhang Y, Wu BX, Metelli A, Thaxton JE, Hong F, Rachidi S, et al. GP96 is a GARP chaperone and controls regulatory T cell functions. *J Clin Invest.* 2015;125(2):859-69.
19. Newton R, Priyadharshini B, and Turka LA. Immunometabolism of regulatory T cells. *Nat Immunol.* 2016;17(6):618-25.
20. Yu X, Teng XL, Wang F, Zheng Y, Qu G, Zhou Y, et al. Metabolic control of regulatory T cell stability and function by TRAF3IP3 at the lysosome. *J Exp Med.* 2018;215(9):2463-76.
21. Zeng H, and Chi H. mTOR signaling in the differentiation and function of regulatory and effector T cells. *Curr Opin Immunol.* 2017;46:103-11.
22. Guo Z, Wang G, Wu B, Chou W-C, Cheng L, Zhou C, et al. DCAF1 regulates Treg senescence via the ROS axis during immunological aging. *Journal of Clinical Investigation.* 2020;130(11):5893-908.
23. Booth DM, Enyedi B, Geiszt M, Varnai P, and Hajnoczky G. Redox Nanodomains Are Induced by and Control Calcium Signaling at the ER-Mitochondrial Interface. *Mol Cell.* 2016;63(2):240-8.
24. Leadsham JE, Sanders G, Giannaki S, Bastow EL, Hutton R, Naeimi WR, et al. Loss of cytochrome c oxidase promotes RAS-dependent ROS production from the ER resident NADPH oxidase, Yno1p, in yeast. *Cell Metab.* 2013;18(2):279-86.
25. Kaminskyy VO, and Zhivotovsky B. Free radicals in cross talk between autophagy and apoptosis. *Antioxid Redox Signal.* 2014;21(1):86-102.
26. Zhang J, Wang X, Vikash V, Ye Q, Wu D, Liu Y, et al. ROS and ROS-Mediated Cellular Signaling. *Oxid Med Cell Longev.* 2016;2016:4350965.
27. Kim HR, Lee A, Choi EJ, Hong MP, Kie JH, Lim W, et al. Reactive oxygen species prevent imiquimod-induced psoriatic dermatitis through enhancing regulatory T cell function. *PLoS One.* 2014;9(3):e91146.
28. Weinberg SE, Singer BD, Steinert EM, Martinez CA, Mehta MM, Martinez-Reyes I, et al. Mitochondrial complex III is essential for suppressive function of regulatory T cells. *Nature.* 2019;565(7740):495-9.
29. Alissafi T, Kalafati L, Lazari M, Filia A, Kloukina I, Manifava M, et al. Mitochondrial Oxidative Damage Underlies Regulatory T Cell Defects in Autoimmunity. *Cell Metabolism.* 2020;32(4):591-604.e7.
30. Maj T, Wang W, Crespo J, Zhang H, Wang W, Wei S, et al. Oxidative stress controls regulatory T cell apoptosis and suppressor activity and PD-L1-blockade resistance in tumor. *Nature Immunology.* 2017;18(12):1332-41.
31. Bhattarai KR, Riaz TA, Kim HR, and Chae HJ. The aftermath of the interplay between the endoplasmic reticulum stress response and redox signaling. *Exp*

Mol Med. 2021;53(2):151-67.
32. Bannykh SI, Nishimura N, and Balch WE. Getting into the Golgi. *Trends in Cell Biology.* 1998;8(1):21-5.
33. Bannykh SI, Rowe T, and Balch WE. The organization of endoplasmic reticulum export complexes. *J Cell Biol.* 1996;135(1):19-35.
34. Hwang SO, Boswell SA, Seo JS, and Lee SW. Novel oxidative stress-responsive gene ERS25 functions as a regulator of the heat-shock and cell death response. *J Biol Chem.* 2008;283(19):13063-9.
35. Cubillos-Ruiz JR, Bettigole SE, and Glimcher LH. Tumorigenic and Immunosuppressive Effects of Endoplasmic Reticulum Stress in Cancer. *Cell.* 2017;168(4):692-706.
36. Lowther DE, Goods BA, Lucca LE, Lerner BA, Raddassi K, van Dijk D, et al. PD-1 marks dysfunctional regulatory T cells in malignant gliomas. *JCI Insight.* 2016;1(5).
37. Ren J, Han L, Tang J, Liu Y, Deng X, Liu Q, et al. Foxp1 is critical for the maintenance of regulatory T-cell homeostasis and suppressive function. *PLOS Biology.* 2019;17(5).
38. Smith PM, Howitt MR, Panikov N, Michaud M, Gallini CA, Bohlooly-Y M, et al. The Microbial Metabolites, Short-Chain Fatty Acids, Regulate Colonic Treg Cell Homeostasis. *Science.* 2013;341(6145):569-73.
39. Sarkar R, Rao KBN, Jha MP, and Mapa K. Endoplasmic reticulum-unfolded protein response pathway modulates the cellular response to mitochondrial proteotoxic stress. *Cell Stress Chaperones.* 2022;27(3):241-56.
40. Carreras-Sureda A, Jana F, Urra H, Durand S, Mortenson DE, Sagredo A, et al. Non-canonical function of IRE1alpha determines mitochondria-associated endoplasmic reticulum composition to control calcium transfer and bioenergetics. *Nat Cell Biol.* 2019;21(6):755-67.
41. Lebeau J, Saunders JM, Moraes VWR, Madhavan A, Madrazo N, Anthony MC, et al. The PERK Arm of the Unfolded Protein Response Regulates Mitochondrial Morphology during Acute Endoplasmic Reticulum Stress. *Cell Rep.* 2018;22(11):2827-36.
42. Gerriets VA, Kishton RJ, Johnson MO, Cohen S, Siska PJ, Nichols AG, et al. Foxp3 and Toll-like receptor signaling balance Treg cell anabolic metabolism for suppression. *Nature Immunology.* 2016;17(12):1459-66.
43. Zhao M, Wang Y, Li L, Liu S, Wang C, Yuan Y, et al. Mitochondrial ROS promote mitochondrial dysfunction and inflammation in ischemic acute kidney injury by disrupting TFAM-mediated mtDNA maintenance. *Theranostics.* 2021;11(4):1845-63.
44. Zeeshan HM, Lee GH, Kim HR, and Chae HJ. Endoplasmic Reticulum Stress and Associated ROS. *Int J Mol Sci.* 2016;17(3):327.
45. Cullinan SB, Zhang D, Hannink M, Arvisais E, Kaufman RJ, and Diehl JA. Nrf2 Is a Direct PERK Substrate and Effector of PERK-Dependent Cell Survival. *Molecular and Cellular Biology.* 2023;23(20):7198-209.
46. Feng Z-z, Luo N, Liu Y, Hu J-n, Ma T, and Yao Y-m. ER stress and its PERK

branch enhance TCR-induced activation in regulatory T cells. *Biochemical and Biophysical Research Communications.* 2021;563:8-14.
47. Eletto D, Chevet E, Argon Y, and Appenzeller-Herzog C. Redox controls UPR to control redox. *Journal of Cell Science.* 2014.
48. Kurniawan H, Franchina DG, Guerra L, Bonetti L, Baguet LS, Grusdat M, et al. Glutathione Restricts Serine Metabolism to Preserve Regulatory T Cell Function. *Cell Metabolism.* 2020;31(5):920-36.e7.
49. Hwang J, and Qi L. Quality Control in the Endoplasmic Reticulum: Crosstalk between ERAD and UPR pathways. *Trends Biochem Sci.* 2018;43(8):593-605.
50. Song M, Sandoval TA, Chae C-S, Chopra S, Tan C, Rutkowski MR, et al. IRE1α–XBP1 controls T cell function in ovarian cancer by regulating mitochondrial activity. *Nature.* 2018;562(7727):423-8.
51. Ma X, Bi E, Lu Y, Su P, Huang C, Liu L, et al. Cholesterol Induces CD8+ T Cell Exhaustion in the Tumor Microenvironment. *Cell Metabolism.* 2019;30(1):143-56.e5.
52. Cao Y, Trillo-Tinoco J, Sierra RA, Anadon C, Dai W, Mohamed E, et al. ER stress-induced mediator C/EBP homologous protein thwarts effector T cell activity in tumors through T-bet repression. *Nature Communications.* 2019;10(1).
53. Rubtsov YP, Rasmussen JP, Chi EY, Fontenot J, Castelli L, Ye X, et al. Regulatory T Cell-Derived Interleukin-10 Limits Inflammation at Environmental Interfaces. *Immunity.* 2008;28(4):546-58.
54. Shan B, Wang X, Wu Y, Xu C, Xia Z, Dai J, et al. The metabolic ER stress sensor IRE1α suppresses alternative activation of macrophages and impairs energy expenditure in obesity. *Nature Immunology.* 2017;18(5):519-29.
55. Xiang H, Tao Y, Jiang Z, Huang X, Wang H, Cao W, et al. Vps33B controls Treg cell suppressive function through inhibiting lysosomal nutrient sensing complex-mediated mTORC1 activation. *Cell Reports.* 2022;39(11).